

**ELECTRODEPOSITION AND CHARACTERIZATION OF Ni-W  
NANOWIRES ON ANODIZED ALUMINUM OXIDE TEMPLATES**

**M.Sc. Thesis by  
Doğın Işıhan PAŞAOĞLU**

**Department : Advanced Technologies**

**Programme : Materials Science and Engineering**

**Thesis Supervisor : Prof. Dr. Mustafa ÜRGEN**

**March 2011**



**ELECTRODEPOSITION AND CHARACTERIZATION OF Ni-W  
NANOWIRES ON ANODIZED ALUMINUM OXIDE TEMPLATES**

**M.Sc. Thesis by  
Doğın Işıhan PAŞAOĞLU**

**Date of Submission : 15.03.2011**

**Date of Defence Examination : 16.03.2011**

**Supervisor (Chairman) : Prof. Dr. Mustafa ÜRGEN (İTÜ)  
Members of the Examining Committee : Prof. Dr. Müzeyyen MARŞOĞLU (YTÜ)  
Assis. Prof. Dr. Kürşat KAZMANLI (İTÜ)**

**March 2011**



**İSTANBUL TEKNİK ÜNİVERSİTESİ ★ FEN BİLİMLERİ ENSTİTÜSÜ**

**ANODİZE ALÜMİNYUM ŞABLONLARA ELEKTROLİTİK KAPLAMA  
YONTEMİYLE Ni-W NANOTELLERİN KAPLANMASI VE  
KARAKTERİZASYONU**

**YÜKSEK LİSANS TEZİ  
Doğan Işhan PAŞAOĞLU**

**Tezin Enstitüye Verildiği Tarih : 15.03.2011**

**Tezin Savunulduğu Tarih : 16.03.2011**

**Tez Danışmanı : Prof. Dr. Mustafa ÜRGEN (İTÜ)  
Diğer Juri Üyeleri : Prof. Dr. Müzeyyen MARŞOĞLU (YTÜ)  
Doç. Dr. Kürşat KAZMANLI (İTÜ)**

**Mart 2011**



## **FOREWORD**

It has been a great pleasure to work with my thesis supervisor Prof. Mustafa ÜRGEN, whom I believe that I have learned so much from him in the way of technical thinking and problem solving. I am thankful to my co-supervisor Ass. Prof. Massimiliano BESTETTI, also Prof. Dr. Gültekin Göller, Ass. Prof. Dr. Kürşat KAZMANLI and Ass. Prof. Dr. Nuri SOLAK for their help and support.

I would like to thank to Res. Assist. Beril AKINCI, Dr. Senem DONATAN and Sinem ERASLAN for their technical support and motivation.

I also would like thank to Fatma BAYATA, Seyhan ATİK, Billur Deniz POLAT for their collaboration and to Talat ALPAK for FEG-SEM and Sevgin TÜRKELI for XRD analyses.

My special thanks goes to my mother Ferda Işık GÜRBÜZTÜRK and my father Gökhan PAŞAOĞLU, who have always believed in me and never hesitated to give me their support not only in this project, but beginning from the day that I was born.

March 2011

Doğan Işıhan PAŞAOĞLU  
Metallurgical and Materials Engineer





## CONTENTS

	<u>Page</u>
<b>FOREWORD.....</b>	<b>v</b>
<b>ABBREVIATIONS .....</b>	<b>ix</b>
<b>LIST OF TABLES .....</b>	<b>xi</b>
<b>LIST OF FIGURES .....</b>	<b>xiii</b>
<b>ÖZET.....</b>	<b>xv</b>
<b>SUMMARY .....</b>	<b>xii</b>
<b>1. INTRODUCTION AND THE AIM OF THE STUDY.....</b>	<b>1</b>
<b>2. NANOWIRES AND THEIR PRODUCTION METHODS .....</b>	<b>5</b>
2.1. Definition of Nanowires.....	5
2.2. Applications of Nanowires.....	6
2.3. Production Methods .....	10
2.3.1. Vapor-Liquid-Solid (VLS) Method .....	12
2.3.2. Laser Assisted Synthesis .....	13
2.3.3. Thermal Evaporation.....	14
2.3.4. Metal-Catalyzed Molecular Beam Epitaxy .....	14
2.3.5. Template-Assisted Synthesis .....	15
2.4. Anodized Aluminum Oxide (AAO).....	15
2.4.1. Anodizing Process.....	17
2.5. Template-Assisted Synthesis Techniques Using AAO.....	21
2.5.1. Pressure Injection .....	21
2.5.2. Vapor Deposition .....	22
2.5.3. Sol-gel Deposition.....	23
2.5.4. Electrochemical Deposition .....	23
<b>3. NI-W ALLOYS AND THEIR ELECTRODEPOSITION .....</b>	<b>33</b>
3.1. Mechanical and Corrosion Properties of Ni-W Alloys .....	33
3.2. Electrodeposition of Ni-W Alloys .....	37
<b>4. EXPERIMENTAL PROCEDURE.....</b>	<b>43</b>
4.1. Surface Preparations.....	44
4.2. Electropolishing .....	44
4.3. Anodizing.....	44
4.4. Pore Bottom Activation .....	47
4.5. Electrodeposition Ni-W nanowires .....	47
4.6. Dissolution of AAO Templates.....	49
4.7. Characterization of Ni-W Nanowires.....	49
4.7.1. XRD Analyses.....	49
4.7.2. FEG-SEM and EDS Analyses.....	49
4.7.2. Polarization Curve Analyses .....	49
<b>5. RESULTS AND DISCUSSIONS .....</b>	<b>51</b>
5.1. Optimization of Anodizing Parameters.....	51
5.1.1. Effect of Surface Finish on the Morphology of AAO .....	51

5.1.2. Pore Size and Thickness of AAO.....	52
5.1.3. Optimization of AAO Substrates for the Production of Ni-W Nanowires.....	59
5.1.4. Electrochemical Dissociation and Zincating.....	60
5.2. Electrodeposition of Ni-W Nanowires .....	62
5.3. Electrocatalytic Properties of Ni-W and Ni-W Nanowires .....	69
<b>6. CONCLUSIONS .....</b>	<b>73</b>
<b>REFERENCES .....</b>	<b>77</b>
<b>CURRICULUM VITAE .....</b>	<b>81</b>

## **ABBREVIATIONS**

<b>AAO</b>	: Anodized Aluminum Oxide
<b>XRD</b>	: X-Ray Diffractometer
<b>FEG-SEM</b>	: Field Emission Gun Scanning Electron Microscope
<b>EDS</b>	: Energy Dispersive Spectroscopy
<b>DC</b>	: Direct Current
<b>μm</b>	: micrometer
<b>nm</b>	: nanometer



## LIST OF TABLES

	<u>Page</u>
<b>Table 1.1:</b> Organizational output share by domains.....	2
<b>Table 2.1:</b> Nanomaterial types and dimension characteristics .....	6
<b>Table 2.2:</b> Nanowire applications .....	6
<b>Table 3.1:</b> Average grain sizes and Vickers microhardness values after electrodeposition in 348°K and annealing in 723°K .....	37
<b>Table 4.1:</b> Operating conditions of electropolishing solution .....	44
<b>Table 4.2:</b> Anodizing parameters .....	46
<b>Table 4.3:</b> Chemical composition of the Ni-W electrolyte .....	48
<b>Table 4.4:</b> Chemical composition of Watts solution .....	48
<b>Table 5.1:</b> Linear assumption of AAO growth rates in different parameters.....	56



## LIST OF FIGURES

	<u>Page</u>
<b>Figure 1.1</b> : The percentage of the spending on nanotechnology applications .....	3
<b>Figure 2.1</b> : An example of Cu/Ni/Fe nanowires .....	5
<b>Figure 2.2</b> : PL spectra of ZnO nanowires below and above lasing threshold .....	8
<b>Figure 2.3</b> : Effect of addition of antibiotin monoclonal antibody .....	9
<b>Figure 2.4</b> : Schematic diagram illustrating the growth of silicon nanowires by the VLS mechanism.....	12
<b>Figure 2.5</b> : An schematic example of an experimental setup for the synthesis of Si nanowires by laser ablation.....	13
<b>Figure 2.6</b> : A simple experimental setup of the thermal evaporation method for synthesizing ZnO nanostructures.....	14
<b>Figure 2.7</b> : A typical MBE growth chamber.....	15
<b>Figure 2.8</b> : Simple scheme of an anodization bath .....	16
<b>Figure 2.9</b> : Schematic view of an AAO template .....	17
<b>Figure 2.10</b> : Elementary processes during pore growth .....	18
<b>Figure 2.11</b> : Current density as a function of time .....	19
<b>Figure 2.12</b> : Current density vs. anodizing time by different voltages.....	20
<b>Figure 2.13</b> : Current density vs. time by different temperatures .....	20
<b>Figure 2.14</b> : Representation of an electrodeposition system .....	24
<b>Figure 2.15</b> : Current vs. time due the nanowire deposition inside the membrane...	25
<b>Figure 2.16</b> : a) reduction and b) oxidation process in A solution.....	26
<b>Figure 2.17</b> : Polarization curves for the alloying elements .....	27
<b>Figure 2.18</b> : Schematic representation of AAO and its barrier layer.....	28
<b>Figure 2.19</b> : Typical current density–time and voltage–time curves by adding re-anodizing in the process .....	29
<b>Figure 2.20</b> : Schematic drawing of controlled dissolution system .....	30
<b>Figure 2.21</b> : Pore opening curve .....	30
<b>Figure 3.1</b> : Tensile strength values vs. elongation curves .....	34
<b>Figure 3.2</b> : Effect of W to the hardness (a) and crystalline size in different temperatures.....	34
<b>Figure 3.3</b> : Potentiodynamic curves in 3.5 wt.% NaCl solution at pH 10 .....	35
<b>Figure 3.4</b> : Potentiodynamic curves in 3.5 wt.% NaCl solution at pH 3 .....	36
<b>Figure 3.5</b> : Ni-W phase diagram.....	38
<b>Figure 3.6</b> : XRD patterns obtained from electrodeposited Ni-W alloys in different pH values .....	39
<b>Figure 3.7</b> : The total W quantity in the Ni-W alloy and W in Ni-W fcc phase as a function of pH.....	39
<b>Figure 3.8</b> : XRD patterns of electrodeposited Ni-W alloys for various current densities .....	40
<b>Figure 4.1</b> : Steps of the experiments.....	43
<b>Figure 4.2</b> : Anodizing system .....	45
<b>Figure 5.1</b> : FEG-SEM image of AAO surface without electropolishing.....	51

<b>Figure 5.2 :</b> FEG-SEM image of electropolished AAO surface .....	52
<b>Figure 5.3:</b> FEG-SEM image of the surface after the etching process at the end of the first step of anodization.....	53
<b>Figure 5.4 :</b> Pore diameters obtained by anodizing at 5°C at a) 30V, b) 50V, c) 70V .....	54
<b>Figure 5.5 :</b> AAO thickness obtained by anodizing at 5°C at a) 30V, b) 50V, c) 70V .	55
<b>Figure 5.6 :</b> Pore diameters obtained by anodizing at 25°C at a) 30V, b) 50V, c) 70V .....	57
<b>Figure 5.7:</b> AAO thickness obtained by anodizing at 25°C at a) 30V, b) 50V, c) 70V .....	58
<b>Figure 5.8 :</b> FEG-SEM image taken after etching.....	59
<b>Figure 5.9 :</b> FEG-SEM image after the second step of anodizing .....	60
<b>Figure 5.10 :</b> a) Barrier layer before electrochemical dissolution, b) after electrochemical dissolution.....	61
<b>Figure 5.11 :</b> a) Cross section view, b) Top view of AAO membrane after zincating .....	62
<b>Figure 5.12:</b> Cell potential vs. time during electrodeposition of Ni.W nanowires ...	63
<b>Figure 5.13:</b> FEG-SEM images of Ni-W nanowires obtained in a)1.87 A/dm <sup>2</sup> and b) 2.18 A/dm <sup>2</sup> .....	62
<b>Figure 5.14:</b> FEG-SEM images of Ni-W nanowires obtained in 1.56 A/dm <sup>2</sup> .....	63
<b>Figure 5.15:</b> FEG-SEM images taken from the top view of deposits a)1.25 A/dm <sup>2</sup> and b) 1.56 A/dm <sup>2</sup> .....	64
<b>Figure 5.16:</b> FEG-SEM images taken from the top view of deposits a)1.87 A/dm <sup>2</sup> and b) 2,18 A/dm <sup>2</sup> .....	
<b>Figure 5.17:</b> EDS patterns of samples deposited in 1.25 A/dm <sup>2</sup> , 1.56 A/dm <sup>2</sup> , 1.87 A/dm <sup>2</sup> and 2.18 A/dm <sup>2</sup> .....	66
<b>Figure 5.18:</b> XRD patterns of Ni-W nanowires a) 1.25 A/dm <sup>2</sup> , b) 1.56 A/dm <sup>2</sup> , c) 1.87 A/dm <sup>2</sup> , d) 2.18 A/dm <sup>2</sup> , e) Ni-W on Al and f) Ni on Al.....	67
<b>Figure 5.19 :</b> Ni-W phase diagram.....	68
<b>Figure 5.20:</b> Polarization curves of electrodeposited Ni and Ni-W on Al.....	69
<b>Figure 5.21:</b> Polarization curve of Ni-W nanowires electrodeposited in 1.56 A/dm <sup>2</sup> .....	70



## **ANODİZE ALÜMİNYUM ŞABLONLARA ELEKTROLİTİK KAPLAMA YÖNTEMİ İLE Ni-W NANO TELLERİN KAPLANMASI VE KARAKTERİZASYONU**

### **ÖZET**

Ni-W alaşımlarının elektrokaplama yöntemiyle üretilmesi ilgi çekici bir konudur. Kaplama sonucu elde edilen ürünler, tribolojik, manyetik, elektriksel ve elektro-erozyon özellikleri açısından benzersiz bir bileşime sahiptir. Bu yöntemle üretilen Ni-W kaplamalar yüksek çekme mukavemeti ve sertlik özelliklerinin yanı sıra, güçlü asitlere karşı yüksek direnci ve yüksek ergime sıcaklığıyla ön plana çıkmakta ve sert krom kaplamalara alternatif olarak görülmektedir. Bu özelliklerin yanı sıra, Ni-W alaşımları, hidrojen çıkışı ve sülfürden arındırma gibi işlemler açısından elektrokatalitik özellikleriyle umut vaad etmektedir.

Bu çalışmanın amacı, grubumuz tarafından daha önceden geliştirilen bir yöntem yardımıyla kendi kendini taşıyabilen Ni-W nanotel üretmek ve karakterizasyon çalışmalarını yürütmektir. Yapılan deneyler, şablon olarak anodize alüminyum oksit (AAO) şablonların, grubumuzca zinkatlama yöntemine dayanan bir metotla aktifleştirilmesi ve doğru akım elektrolitik kaplama yöntemi ile AAO şablonlara Ni-W nanotel kaplanmasına dayanmaktadır. Kaplama devam ettirildikçe porlar Ni-W nanoteller ile doldurulmakta ve ardından AAO ve Al katmanları çözülerek geriye kendi kendini taşıyabilen nanoteller kalmaktadır.

Ni-W nanotellerin üretimi için öncelikle AAO şablonların üretimi optimize edilmiştir. Önceden tavlanan ve elektro parlatma işlemine tabi tutulan saf alüminyum numuneler, okzalik asit ile iki basamaklı anodizasyon basamaklarından geçirilmiş; yaklaşık 100 nm por çapı elde edilmiştir. Anodizasyon süresi ayarlanarak kalınlık 2 µm elde edilmiştir. Elde edilen porlu yapının tabanları elektrokimyasal ayrışma ve zinkatlama yöntemi ile doğru akım elektrolitik kaplama için hazır hale getirilmiştir. Elektrolitik kaplama deneyleri 1.25 A/dm<sup>2</sup>, 1.56 A/dm<sup>2</sup>, 1.87 A/dm<sup>2</sup> ve 2.18 A/dm<sup>2</sup> değerlerinde gerçekleştirilmiştir. Atomik %9 W içeren Ni-W alaşım eldesi için optimizasyonlar yapılmış; kullanılan çözeltinin kritik pH ve kaplama anındaki akım yoğunluk değerleri ortaya çıkarılmıştır. Deneylerin sonunda, uzunlukları 1.5-1.8 µm ve çapları ortalama 120 nm ile 140 nm arası değişen Ni-W nanoteller başarı ile üretilmiştir. Elde edilen numuneler Watts çözeltisi ile kalınlaştırılmış ve ardından AAO ve Al katmanları NaOH çözeltisinde çözülmüştür; kendi kendini taşıyan Ni-W nanoteller üretilmiştir. Ardından FEG-SEM ve XRD analizleri yapılmış, elektrokatalitik özellikleri polarizasyon eğileri üzerinden incelenmiş ve Ni-W nanotellerin düz elektrolitik Ni kaplamalara göre davranışı irdelenmiştir. Deney sonuçları, yapı içine oksit katılımı engellenebilirse Ni-W nanotellerin elektrokatalitik malzeme olarak kullanılabilme potansiyeline sahip oldukları göstermiştir. Bu üretim yöntemi sayesinde ilk defa kendi kendini taşıyabilen Ni-W nanotel yapılar üretilmiştir; ve yüksek yüzey alanları nedeniyle kullanım alanlarının genişleyeceği düşünülmektedir.



# **ELECTRODEPOSITION AND CHARACTERIZATION OF Ni-W NANOWIRES ON ANODIZED ALUMINUM OXIDE TEMPLATES**

## **SUMMARY**

The electrodeposition of Ni-W alloys is an interesting subject due to the unique properties of the final products such as the combination of tribological, magnetic, electrical and electro-erosion properties. They exhibit high tensile strength and hardness properties, high resistance to strong acids and have high melting temperature. They are also considered as alternative for hard chromium coatings. Besides these properties Ni-W alloys are promising materials for electrocatalytic applications such hydrogen evolution, desulphurization.

The aim of this study was to produce free standing Ni-W alloy nanowires with a previously developed method in our group and to conduct characterization analyses. The method is based on using anodized aluminum oxide (AAO) as templates. With a special method based on zincating that was developed within the group, the bottoms of the pores of the prepared AAO templates are activated. By this process the AAO templates become ready for filling the pores with metal using DC electroplating. By continuing the electrodeposition after filling of the pores, the wires within the pores are covered by a layer of the same metal. This layer supported the wires after dissolving away the AAO and aluminum creating an easily handled free standing structure.

For the production of Ni-W nanowires the parameters of the AAO template formation was optimized. After two step anodization of annealed and electropolished pure aluminum in oxalic acid solutions well ordered pores around 100 nm in diameter was obtained. The length of the pores was adjusted to 2  $\mu\text{m}$  by tuning the anodization time. This porous structure was pore bottom activated with a method based on electrochemical dissociation and zincating that allowed the DC electrodeposition starting from pore bottoms. The samples were electrodeposited in 1.25 A/dm<sup>2</sup>, 1.56 A/dm<sup>2</sup>, 1.87 A/dm<sup>2</sup> and 2.18 A/dm<sup>2</sup>. After optimization of Ni-W alloy deposition for obtaining 9 at% W in the deposit pore filling experiments were conducted revealing the need of further optimization for achieving a successful electrodeposition within the pores. The critical role of solution pH and deposition current density was revealed. At the end of the experiments, Ni-W nanowires with the length of 1.5-1.8  $\mu\text{m}$  and diameters ranging from 120nm to 140 nm were produced. After thickening the Ni-W coated layer with Watts solution and dissolving the AAO and Al layers of the samples in NaOH solution, free-standing Ni-W nanowires were obtained. FEG-SEM, XRD analyses were performed and polarization curves for electrocatalytic activity were investigated. It was demonstrated that Ni-W nanowires have a potential to be utilized as electrocatalysts if oxide formation in the structure is avoided. This method of production introduced is the first study that showed the possibility of the production of free standing Ni-W structures with the said method and believed to extend the high surface area related applications, such as catalysis, of these alloys.



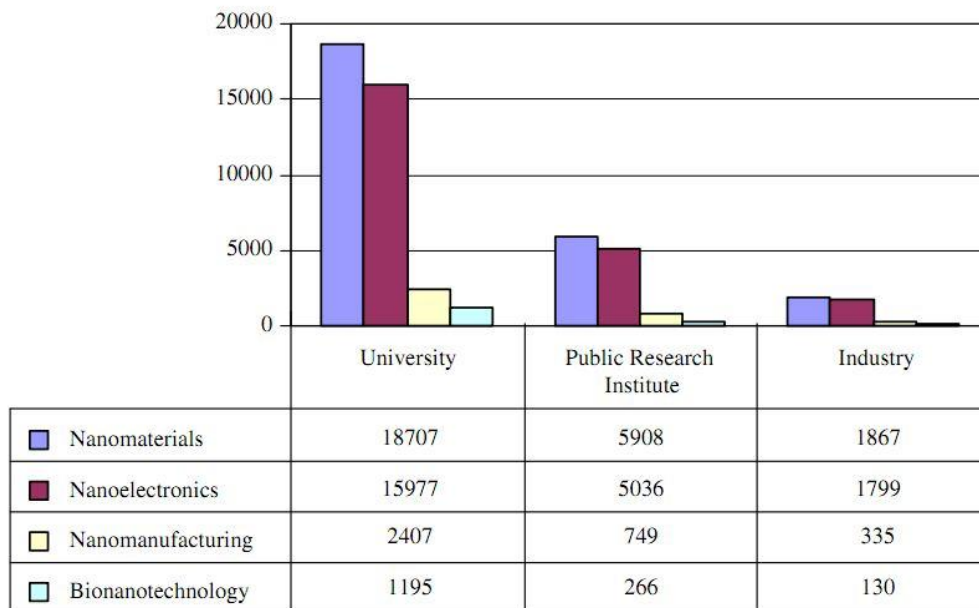
## 1. INTRODUCTION AND THE AIM OF THE STUDY

Nanotechnology is an advanced technology involving the fabrication and use of devices so small that the convenient unit of measurement is nanometers. This technology, which is being used since the ancient times, continues to surprise researchers nowadays with every single unveiled findings.

The “modern” journey of nanotechnology can be traced back to 1857, Michael Faraday, who made some experiments on nanomaterials for the first time. He synthesized gold particles by reducing chloroauric acid; in which as a result, he obtained ruby-red and pink color dispersion of gold particles. These were probably the first colloidal particles reported in the literature. In 1914, Richard Adolf Zsigmondy, made some research about gold solutions and other nanomaterials with sizes less than 10 nm, which also obliged him to express “nanometers” and determined the term as  $1/10^6$  of a millimeter. In 1959, famous physicist Richard Feynman gave a talk titled “There’s Plenty of Room at the Bottom”, in which he hypothesized that atoms and molecules could be manipulated like building blocks. This way of thinking inspired lots of scientist all over the world. In 1974, Norio Taniguchi used the term “nanotechnology” for the first time in the literature. Also in 1974, monolayer of atoms were deposited on a substrate for the first time by Dr. Tuomo Suntola in Finland. Gerd Binnig and Heinrich Rohrer, two developers in IBM Zurich Laboratories, invented Scanning Tunneling Microscope (STM) in 1981 and won Nobel Prize in 1986. In 1989, the scientists in IBM managed to manipulate atoms in a desired way by creating a writing of “IBM” of 35 xenon atoms, which was considered as a great success (Url 1,Url 2).

Nanotechnology research is being developed nowadays mainly in universities and public research institutes in an interdisciplinary way, which combines many branches such as chemistry, physics, materials science and biology. The intention is to understand and utilize nanoscience for scientific curiosity and use it through government initiative drives or industry (Islam, 2010). Table 1.1 below shows the output shares changing according to the domains.

**Table 1.1:** Organizational output share by domains (Islam, 2010)



It was estimated that, the number of global researchers and workers were around 400,000 in 2008 and 150,000 of them were from the United States. Another prediction in 2000 stated that there will be around 2 million people all around the world working on nanomaterials also depending on its market demand. Until 2008, the number of patent applications were around 13,000; which 3,729 of them were filled at United States Patent and Trade Office. This is an accelerated trend (annual increment of 35%) if the total number of 12,000 and 405 patents in the US in 2000 are considered.

According to the research claimed by Roco, the market is doubled every three years especially as the new nanotechnological products are presented. The total estimated value of nanotechnology products was around \$200 billion worldwide; which \$80 billion was from the US in 2008 (Roco, 2010). Figure 1.1 shows the percentage of the spending on nanotechnology applications.

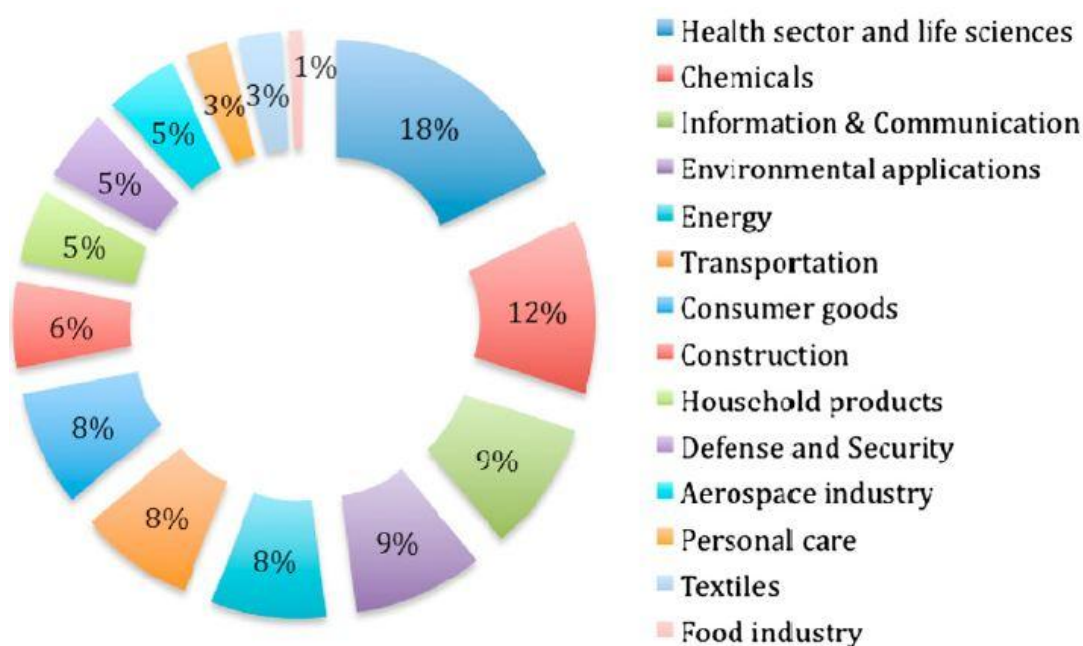


**Figure 1.1:** The percentage of the fund spent on nanotechnological applications (Delgado, 2010)

\$15 billion investment by private and public sources were made in 2008, which \$3.7 billion belonged to the US. The Federal Government of the country supplied \$1.55 billion. If the venture capital funds are investigated, the amount of investment was around \$1.4 billion in 2008; whereas in 2009 the funds were decreased by 40% due to the economical crisis (Roco, 2010).

It is known that there are many different types of nanomaterials serving different needs which are being used many different areas, with respect to their uniquely high surface to volume ratios. For instance, a 30 nm iron particle has 5% of atoms on the surface, whereas a 3 nm particle has 50% of atoms on the surface; which makes the surface phenomena crucial unlike the bulk form of iron. Properties like adsorption, solubility, reactivity, catalysis and many more depend on the size of the particles (Meyyappan, 2010).

There have been many attempts in the recent years on growing nanowires in specific dimensional aspect ratios with respect to their unique physical and mechanical properties depending on the materials they are composed of. These materials are generally metals/metallic alloys or semiconducting materials serving different uses. The applications of nanowires varies from solar cells to LEDs and biological sensors (Meyyappan, 2010).

Ni-W alloys show a unique combination of properties due to their higher strength and hardness, improved tribological resistance, thermal properties such as high melting point, hot strength, oxidation resistance; as well as electrocatalytic and better corrosion properties when compared to elemental Ni (Krolikovski, 2009; Mitov, 2008). Ni-W alloys have a potential to be used for the hydrogenation process to lower the aromatic content in diesel fuels, removal of organo-sulfur contaminants and desulfurization in water treatment process (Sheng, 2010; Vradman, 2001; Mitov, 2008).

There are many different methods available for synthesizing nanowires such as vapor-liquid-solid (VLS) method, thermal evaporation, metal-catalyzed molecular beam epitaxy and template-assisted synthesis. These methods will be explained briefly in the next chapters of the study. Among these methods, template-assisted synthesis method is a very significant and versatile method and includes different types of nanowire deposition techniques including pressure injection, vapor deposition, sol-gel deposition and electrodeposition. In the present study, template-assisted study was selected for Ni-W nanowire production. Literature consists of many different materials utilized as membranes for nanowire deposition. The templates are generally made of anodic alumina (AAO), nano-channel glass, ion track-etched polymers or mica films. AAO templates however, are the most common templates utilized with respect to their ease of production, optimization and their well-organized pore structure. In the present work, anodizing parameters were examined, optimized and modified with surface finishing techniques developed by our surface technologies laboratories for sufficient Ni-W nanowire deposition. Among the nanowire deposition techniques, electrodeposition was utilized due to its cost effective properties and ease of parameter adjustments which makes the method useful for obtaining nanowires with diverse properties (Wagner, 1967; Shankar, 2005; Cao, 2007; Wang, 2008; ).

The aim of the study was to develop an optimized method for Ni-W nanowire electrodeposition on AAO templates and investigate their electrocatalytic properties after performing characterization analyses.



## 2. NANOWIRES AND THEIR PRODUCTION METHODS

### 2.1 Definition of Nanowires

Nanowires are defined as extremely thin wires in the order of  $10^{-9}$  meters and are very challenging for scientists for nanoscience studies and nanotechnology applications. Physically, they have two limited quantum directions and one unconfined direction for uses like electrical conduction. The density of electronic states in the structure gives them different optical, electrical and magnetic properties when compared to bulk states. Besides these properties, nanowires can also be useful in some limited applications which cannot be supplied by bulk counterparts and can be modified nonlinearly in small diameter nanowires (Url 3, Bhushan, 2004). Figure 2.1 shows an SEM image of Cu/Ni/Fe nanowires and table 2.1 illustrates the types of nanomaterials including nanowires due to their dimensions.

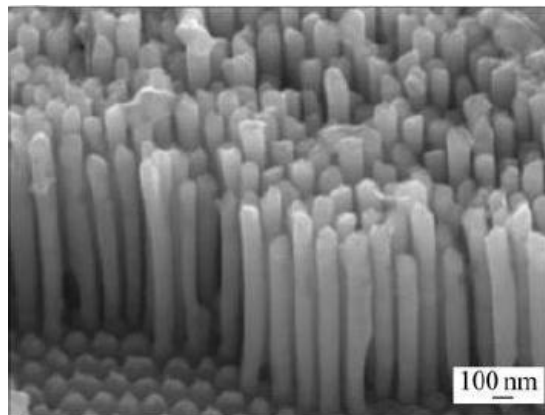


**Figure 2.1:** An example of Cu/Ni/Fe nanowires (Hamrakulov, 2009)

**Table 2.1:** Nanomaterial types and dimension characteristics (Salamon, 2010)

Type of Nanomaterial	Number of dimensions and size
Nanoparticle	Three dimensions in the 1 to 100 nanometers (nm) range
Nanotubes/nanowires	Two dimensions in the 1 to 100 nm range
Nanofibers	Length ranges between 50 nm and 300 nm with diameter <50 nm
Nanofilms	One dimension in the 1 to 100 nm range
Nanoplates	Two dimensions in the 1 to 100 nm range

## 2.2 Applications of Nanowires

There have been many attempts in the recent years on growing specific nanomaterials in one dimension due to their unique properties. If the diameter of the nanowires are less than bohr radius, the electron transport properties, band structure and optical properties drastically change. In table 2.2, some examples for nanowire applications are given. (Meyyappan, 2010).

**Table 2.2:** Nanowire applications (Meyyappan, 2010)

Material	Application
Silicon	Electronics, biosensors, solar cells
Germanium	Electronics, IR detectors
Tin oxide	Chemical sensors
Indium oxide	Chemical sensors, biosensors
Indium tin oxide	Transparent conductive film in display electrodes, solar cells, organic light-emitting diodes (LEDs)
Zinc oxide	UV lasers, photodetectors, UV LEDs, field emission device
Vanadium oxide	Chemical sensor
Gallium nitride	High-temperature electronics, UV detectors and lasers, automotive electronics, sensors
Boron nitride	Insulator
Gallium arsenide	Electronics
Indium phosphide	Electronics, optoelectronics, lasers
Zinc selenide	Photonics (Q-switch, blue green laser diode, photodetectors)
Indium selenide	Phase change memory device
Germanium telluride	Phase change memory device
Cadmium telluride	Solar cells
Copper, tungsten	Interconnects
Gold, silver	Biosensors

The last three decades has been a great period of time for silicon devices. Silicon nanowires have been reported to be produced for n-type and p-type field effect

transistors (FET) by different techniques. SiNW is fabricated for FET with epitaxial source and drain contacts. On the other hand, vertical sound gate transistors (VSGT) are becoming more popular in the last two decades, which is very advantageous compared to other types of transistors. In order to produce VSGT, ZnO nanowires are grown as a channel material on a doped SiC substrate by vapor-liquid-solid method (VLS). Germanium is another preferred element due to its higher electron, hole mobilities and larger Bohr radius compared to silicon for n-type and p-type FET. Ge nanowires are grown on SiO<sub>2</sub> substrates with In as a catalyst. Then GeNOI FET is produced by photolithography patterning and metal lift-off process. GaN nanowires are semiconductors with a wide band gap enabling themselves for high temperature applications. Back-gated GaN nanowires having diameters between 90-200 nm are used as depletion mode transistors. A great amount of negative potential difference is need to be applied with respect to the backgating configuration and thick oxide layers to be turned off. For VSGT systems, InAs or InP channels can be preferred, which are produced by molecular beam epitaxy method. For memory devices, InO<sub>2</sub> nanowires were used but the molecules themselves have the possibility to be unstable at elevated temperatures. SiNW can be fabricated for durable nonvolatile memory supplying reversible read, write and erase properties. The utilization of GaN nanowires is another alternative for SiNW nanowires, which are also superior due to their radiation hardness in aggressive environments. Phase change random access memories (PRAM) are another types of devices that nanowires are utilized. It consists of a thin layer of phase changing material (PCM) which is in between two pair of electrodes. The resistance of PCM changes between amorphous and crystalline states by the applied pulse. These two phases represent two logic states. GeTe nanowires can be used for PRAMs. According to the experimental results of In<sub>2</sub>Se<sub>3</sub> nanowires show better results that GeTe dur to its higher resistivity (Meyyappan, 2010).

The optoelectronic properties of nanowires are also a great issue of interest. Light emission from nanowires can be observed by photo-luminescence (PL) or electroluminescence (EL) depending on the electronic excitation by optical illumination or through p-n junction. Photodetectors, light emitting diodes (LED), nanoscale lasers, photovoltaic cells and many other devices can be made of nanowires. A photodiode is basically a p-n junction. An optical input creates

electrons and holes (carriers) in the high field region with fast response time, high sensitivity and high signal-to-noise. With these properties, photodetectors are preferred more than photoconductors. It was claimed that silicon nanowire FETs can also be used similar to the back-gated devices due to their photoconductance response. Oxide nanowires having a large energy gap between the conduction and the valance band such as  $\text{Ga}_2\text{O}_3$  exhibits photocurrent behavior in the UV region and extremely low free carrier density, short response time and recovery time, which makes it superior to ZnO and  $\text{In}_2\text{O}_3$ . Figure 2.2 shows the PL spectra of ZnO nanowires below and above lasing threshold. Light emitting diodes (LEDs) are very popular in the areas of lighting, displays and other applications. GaN, ZnO and InP were examined for their applicability in LEDs. Doping GaN with Mg turns the n-type GaN into a p-doped semiconductor. Array of nanorods can also be fabricated consisting of multiple quantum wells (MQM), such as GaN/InGaN nanowires. Nanowires can also be used as nanoscale lasers since the diameter can be smaller than the emission wavelength and their ability to create optical cavities. ZnO were successfully fabricated as a UV laser by VLS method. GaN UV lasers were also produced according to the literature obtained. As for near-infrared lasers, GaSb nanowires can be fabricated by spontaneous nucleation technique which will not be mentioned in detail here (Meyyappan, 2010; Bhushan 2004).

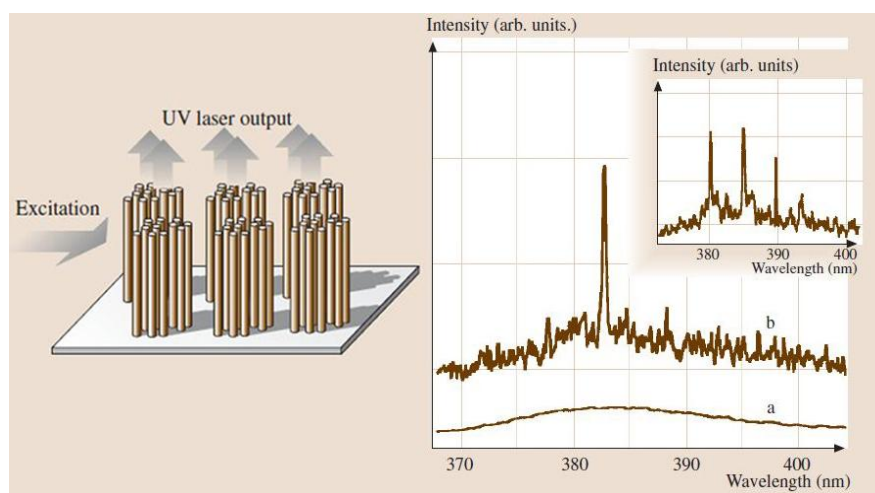


**Figure 2.2:** PL spectra of ZnO nanowires below and above lasing threshold  
(Bhushan. 2004)

It is known that many materials change their various properties by being affected by the environment. This interaction utilizes specific materials enabling them to be used

as sensors. For instance, when single-walled carbon nanotubes (SWNTs) are exposed to certain gases or vapors, their resistance, capacitance and dielectric constant change. A similar effect can also be observed in metal oxides. Biomolecules containing amino, nitro groups or deoxyribonucleic acid (DNA) can be used with inorganic nanowires for biosensing (Meyyappan, 2010).

Basically, sensors can be divided into two: Chemical sensors and biosensors. Chemical sensors can be used in many sectors in industry such as chemistry, security, biomedical, mining, agriculture, food industry etc. Nanosized materials are advantageous when compared to bulk materials. Increased sensitivity and response time two significant properties for nanowires. So far, there have been studies on nanowires made of ZnO, SnO<sub>2</sub>, In<sub>2</sub>O<sub>3</sub>, V<sub>2</sub>O<sub>5</sub>, GaN and silicon for chemical sensors. The sensing mechanism begins with the adsorption of oxygen on the surface of oxide nanowire surface and form O<sub>2</sub><sup>-</sup> and O<sup>-</sup>. Since the electrons on the surface are spent for the ion formation, the resistance state increases. In these conditions, when the surface interacts with a reducing gas, electrons are released back and the conductivity increases. For the case of oxidizing gases such as NO<sub>2</sub>, the resistance increases even more and negatively charged forms are observed in the surface. As for biosensors, the number of research is less than what has been done for chemical sensors. Si nanowires as well as Au and Pt were successfully fabricated for the detection of DNA, virus, cholesterol, prostate-specific antigens (PSA), glucose, cytokeratin in cancer diagnosis and foodborne pathogens. It is known that stratavidin molecules can bind to silicon nanowires functionalized with biotin and when the binding takes place, the resistance of the nanowires changes. Figure 2.3 shows the effect of addition of antibiotin monoclonal antibody in a buffer solution containing silicon nanowires functionalized with biotin in region two (Meyyappan, 2010; Bhushan,2004).

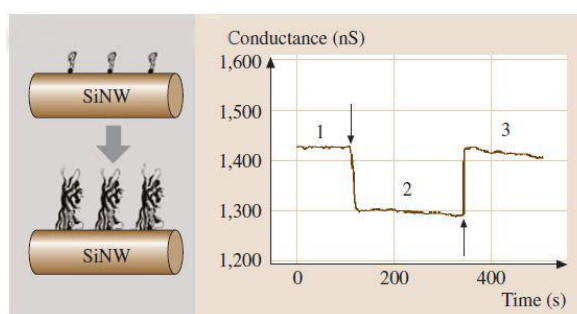


**Figure 2.3:** Effect of addition of antibiotin monoclonal antibody (Bhushan, 2004)

Energy sector is another sector that nanowires can be useful for. One dimensional structures such as nanowires and nanotubes have direct channels for charge transport, which decreases the energy loss. Inorganic nanowires can be utilized for solar cells and electrochromic devices. Dye sensitized solar cells (DSSCs) are alternative type of solar cells to traditional p-n junction type cells and preferred due to their low cost. Most of the nanowires serving for solar cells are mostly in this class. DSSC solar cells uses semiconducting nanostructures having wide bandgap and a monolayer dye covering it, enabling visible light absorbance. The nanoparticle-based films on DSSCs are not well-structured structures and charge transport can be slowed down. Nanowires are utilized to improve the charge transport dynamics of the films. Therefore, longer nanowires can even be used for increasing the absorption minimizing charge loss.  $\text{TiO}_2$ ,  $\text{ZnO}$  and  $\text{Nb}_2\text{O}_5$  nanowires are some examples for DSSC solar cell applications. Another application for nanowires is in electrochromic devices (EC). EC devices are made of materials that change their optical properties when a small electric field is applied. Nanowires used in these devices enable faster charge transport that lets faster color switch and higher color contrasts.  $\text{WO}_3$  and  $\text{V}_2\text{O}_5$  are two examples that have been studied for EC devices (Meyyappan, 2010).

## **2.3 Production Methods**

There are many different ways suggested in the literature for synthesizing nanowires and are classified depending on the technology used or to the growth mechanism of the nanowires.

Generally, the production methods can be classified into five main categories:

- Vapor-Liquid-Solid (VLS) Method for Synthesis
- Laser Assisted Synthesis
- Thermal Evaporation
- Metal-catalyzed Molecular Beam Epitaxy
- Template-Assisted Synthesis

Table 2.3 below shows some examples of the synthesis methods that are used for selected materials for nanowire production.

**Table 2.3:** Synthesis methods for some nanowires. a) Electrochemical Deposition, b) VLS method, c) Chemical Vapor Deposition, d) Organometallic chemical vapor deposition (Bhushan, 2004)

Material	Growth Technique
Ag	DNA-template, redox template, pulsed ECD <sup>a</sup>
Au	template, ECD <sup>a</sup>
Bi	stress-induced template, vapor-phase template, ECD <sup>a</sup> template, pressure-injection
Bi <sub>2</sub> Te <sub>3</sub>	template, dc ECD <sup>a</sup>
CdS	liquid-phase (surfactant), recrystallization template, ac ECD <sup>a</sup>
CdSe	liquid-phase (surfactant), redox template, ac ECD <sup>a</sup>
Cu	vapor deposition template, ECD <sup>a</sup>
Fe	template, ECD <sup>c</sup> shadow deposition
GaN	template, CVD <sup>c</sup> VLS <sup>b</sup>
GaAs	template, liquid/vapor OMCVD <sup>d</sup>
Ge	high-T, high-P liquid-phase, redox VLS <sup>b</sup> oxide-assisted
InAs	template, liquid/vapor OMCVD <sup>d</sup>
InP	VLS <sup>b</sup>
Mo	step decoration, ECD <sup>a</sup> + redox
Ni	template, ECD <sup>a</sup>
PbSe	liquid phase
Pd	step decoration, ECD <sup>a</sup>
Se	liquid-phase, recrystallization template, pressure injection
Si	VLS <sup>b</sup> laser-ablation VLS <sup>b</sup> oxide-assisted low-T VLS <sup>b</sup>
Zn	template, vapor-phase template, ECD <sup>a</sup>
ZnO	VLS <sup>b</sup> template, ECD <sup>a</sup>



### 2.3.1 Vapor-Liquid-Solid (VLS) Method

Vapor-liquid-solid method is being used in the recently years for anisotropic crystal structured semiconductor nanowires. The production method is based on taking a source material in gas phase and have it absorbed by turning into a liquid droplet of catalyst. The method was first used for the the growth of single crystal silicon whiskers with a diameter ranging from 100 nm to microns; and a molten particle of gold was used on silicon substrate. According to the suggested mechanism, the source material precipitates as solid by the supersaturation of the liquid alloy. Then this precipitate acts as a seed for more deposition on a preferred site. Therefore, the elongation of the seed into nanowire, even into a whisker is done by anisotipically as sketched in figure 2.4 .The final products are of high purity, with the solidified catalyst on the top of nanowires (Wagner, 1967).

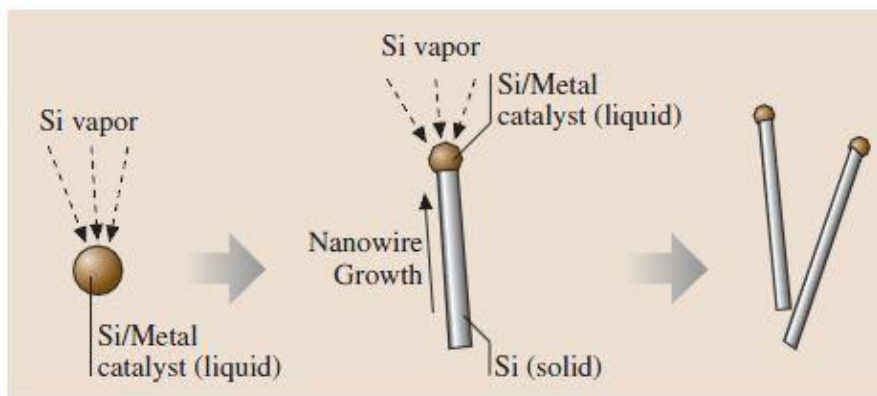


**Figure 2.4:** Schematic diagram illustrating the growth of silicon nanowires by the VLS mechanism (Bhushan, 2004)

Since VLS method is simple with its growth mechanism, the technique requires expensive experimental setup when compared to other convenient methods. Moreover, the growth of nanowires is limited for the use of materials that can form eutectic with catalysts at growth temperature and to simple oxides. Due to the high melting temperature of most of the oxides, the system also needs high temperatures to be operated. Special catalysts are need for nanowire growth which creates difficulties on removing these capsules from the tip of the nanowires (Shankar, 2005, Cao, 2007).



### 2.3.2 Laser Assisted Synthesis

Just like VLS, the mechanism is also based on nucleation and growth of nanowires by a critical catalyst but by this time with laser, in laser ablation method. The use of laser primarily gives the advantage of synthesizing nanowires with complex chemical compositions. Moreover, the target or the source material does not have to be crystalline and simply mixing the elements is enough for the setup. Figure 2.5 represents the system. After the setup is finished, laser ablates the materials in a very short time into vapor phase and then nucleated and grown on the surface of the substrate. Short time ablation is a non-thermo equilibrium process which is called congruent evaporation. It can be noted that this method is useful for materials that need to be synthesized in high temperatures or for doping nanowires. It was reported that laser ablation can be replaced with CVD for ZnO nanowire production due to the final porous structure obtained by CVD. The atmosphere of the chamber in the system can be arranged due to the structure that is aimed to be obtained (Wang, 2008).

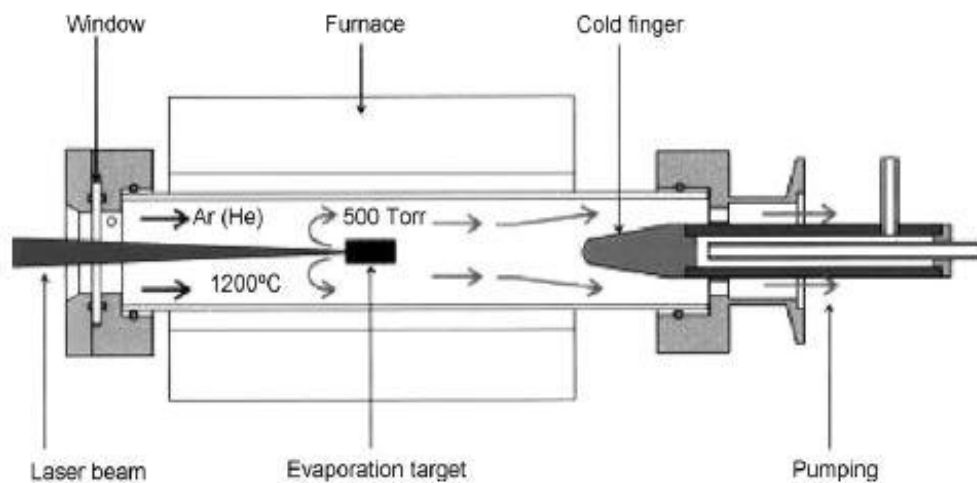


**Figure 2.5:** A schematic example of an experimental setup for the synthesis of Si nanowires by laser ablation (Wang, 2008)

By laser ablation, it is possible to produce nanowires in the range of 10-50  $\mu\text{m}$  in length and diameters smaller than 10 nm. When compared to VLS, larger amounts of smaller nanoparticles of metals or metal silices can be produced by laser ablation at high temperatures and without any need for a catalyst (Wang, 2008). It can be asserted that this method is faster but needs more energy than the other methods, which is a great drawback.

### 2.3.3 Thermal Evaporation

Another method for nanowire synthesis is thermal evaporation. The source materials (generally metal oxide powders) are carried in the system by the atmosphere, and as they are transferred, condensation takes place on the substrate due to the temperature gradient (figure 2.6). There are mainly two parameters that are very important in the system: The temperature and vacuum conditions. This fabrication is generally used for metal oxides, such as ZnO, SnO<sub>2</sub>, In<sub>2</sub>O<sub>3</sub>, VO, etc. and some semiconductors. The chamber may work under vacuum or in inert gasses. The nanowires are produced without any need for catalyst, directly from the vapor (Wang, 2008).

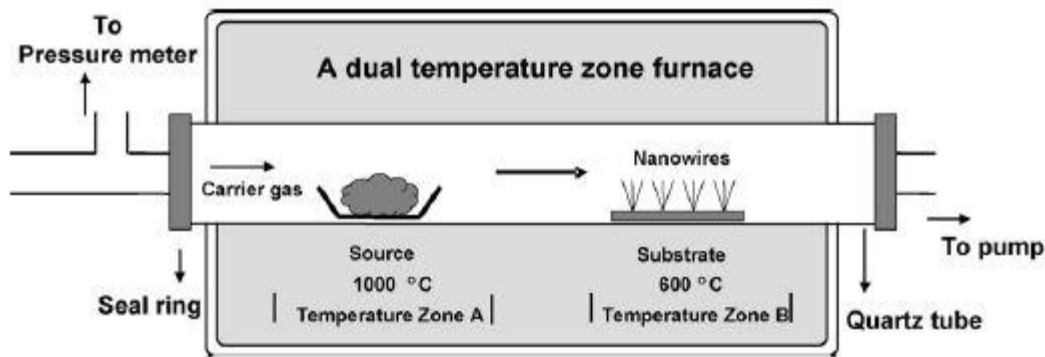


**Figure 2.6:** A simple experimental setup of the thermal evaporation method for synthesizing ZnO nanostructures (Wang, 2008)

### 2.3.4 Metal-Catalyzed Molecular Beam Epitaxy

Metal-catalyzed molecular beam epitaxy, is technique that uses ultra high vacuum conditions. In this method, the beam of atoms (source) are evaporated from the effusion cells and are transported directly to the substrate. In VLS, in order to have the catalytic decomposition of precursors, metal particles are needed. In MBE however, there are no precursors needed. The correct preparation of the substrate surface is very important in order to obtain good quality of nanowires. The ultra high vacuum is useful for eliminating the contamination or the oxidation that might be encountered on the material surface. On the other hand, low growth temperature is a plus, when VLS, laser ablation and thermal evaporation is considered. The growth parameters can be adjusted separately. Figure 2.7 below shows a typical MBE growth chamber (Wang, 2008).

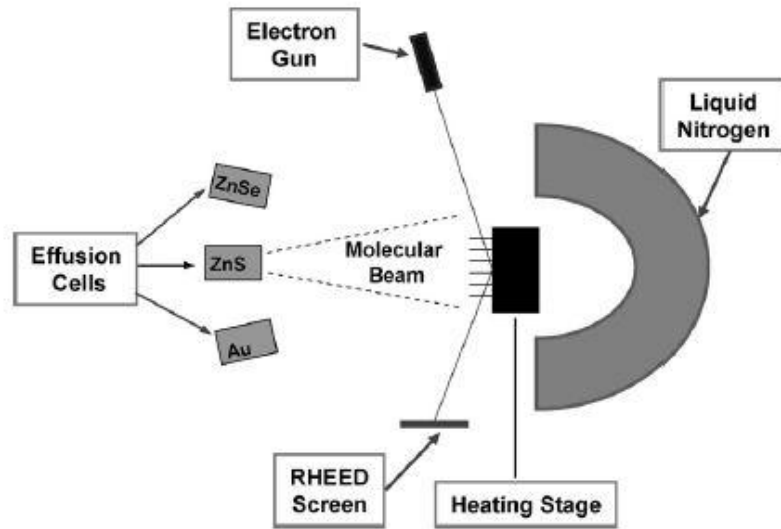


**Figure 2.7:** A typical MBE growth chamber (Wang, 2008)

### 2.3.5 Template-Assisted Synthesis

Until now, the productions methods described above need specific equipment setups and generally expensive for nanowire production. Template assisted synthesis has gained great attention in the recent years for nanowire synthesis due to its simplicity. The method is based on synthesizing a porous template and then eliminating it after the filling of templates with the material desired for nanowires gaining the pore morphology. The templates are generally made of anodic alumina (AAO), nano-channel glass, ion track-etched polymers, or mica films. Among those materials, anodic alumina (AAO) is the most popular type of template primarily due to its pore formation in uniform diameters, uniform pore distribution and its high temperature durability (Bhushan, 2004). This method will be explained further with its varied applications.

### 2.4 Anodized Aluminum Oxide (AAO)

The history of electrochemical oxidation of aluminum traces back to the first years of the last century; yet nowadays anodizing is mostly used for its protective and decorative coating properties. This trend also gave a rise to the patent applications after the year 1950's. In 1923, Bengough and Stuart, applied for the patent in anodic process for Al and its alloys for anti-corrosion. Carboni, invented a coloring method by applying AC on metal salt solution right after sulfuric acid anodizing in 1936., which is a commonly used process. In 1953, Keller and his friends, had the chance to

have a closer look at the anodized alumina and explained the structure consisting of a hexagonal porous layer and a barrier layer; which can be considered as a giant step for understanding the physical and chemical properties of AAO (Alpay, 2009).

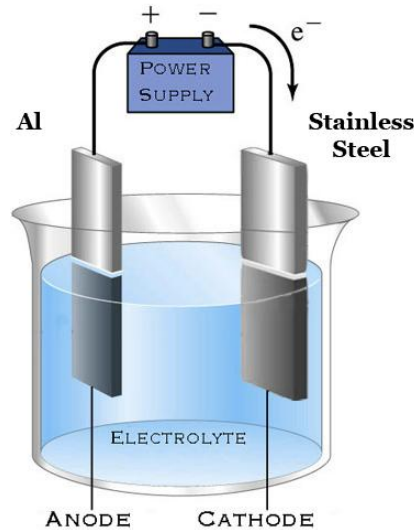


**Figure 2.8:** Simple scheme of an anodization bath (Url-6)

During anodizing, the surface of aluminum is coated with porous aluminum oxide as a result of an electrochemical process in an acidic solution. The diameters obtained are uniform with respect to the balance between diffusion and dissolution of the alumina in the electrolyte (figure 2.8). The ordered hexagonal structure of pores is formed by the stress in the interface layer between aluminum and alumina, driven by the volume expansion. Therefore the pores have hexagonal shapes by repulsive forces. Chromic acid, oxalic acid, phosphoric acid, boric acid, sulfuric acid, sulfuric/oxalic acid or some organic acids can be preferred as an acidic solution for anodizing. By changing the anodization conditions, a wide range from less than 10nm to 200 nm of pore diameter can be obtained with the pore density of  $10^9 - 10^{11}$  pore/cm<sup>2</sup> (Bhushan, 2004; Hecker, JR. J. C., nd; Shankar, 2005).

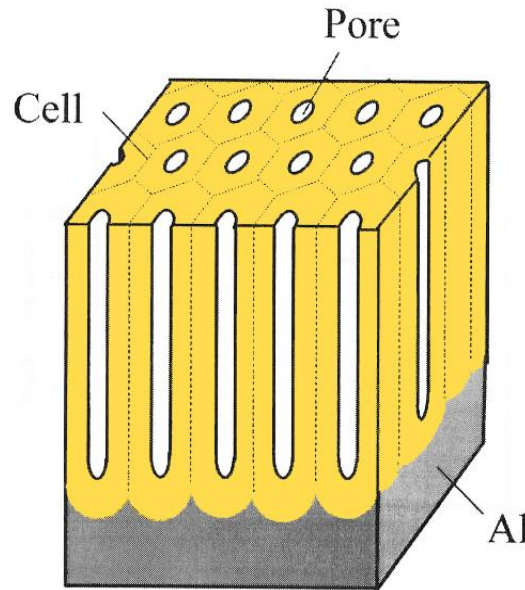


**Figure 2.9:** Schematic view of an AAO template (Url-4)

#### 2.4.1 Anodizing Process

When the Al is anodized,  $O_2$  evolution takes place on the anode and the oxygen covers the anode and AAO is formed. It should be noted that the mechanism of the anodizing does not take place on the outer surface, but on interchange surface between aluminum and aluminum oxide. Briefly, when the aluminum contracts with the electrolyte, a protective layer is formed. Then surface fluctuations cause local field distributions and the pores are created. Finally the pores grow depending on the environment conditions supplied. The pores grow perpendicular to the aluminum surface. The barrier thickness, pore diameter and the interpore diameter is directly related to the voltage applied. The oxide growth at the metal/oxide interface mainly controls the barrier layer thickness and depends on the migration of oxygen containing ions  $O^{2-}/OH^-$  from the electrolyte. At the same time, oxide layer is dissolved by the migration of  $Al^{+3}$  ions to the electrolyte (figure 2.10). In summary, two mechanisms work opposite to each other (Alpay, 2009; Bandyopadhyay, 2003).

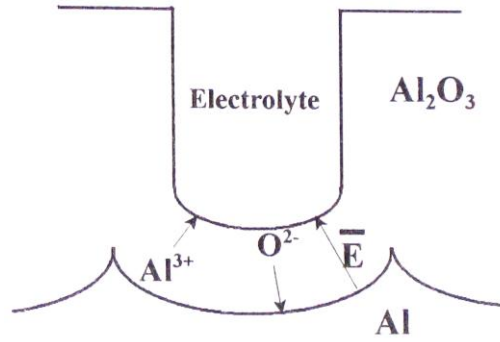
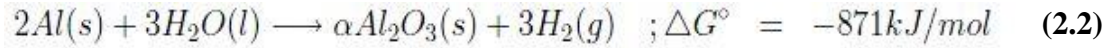
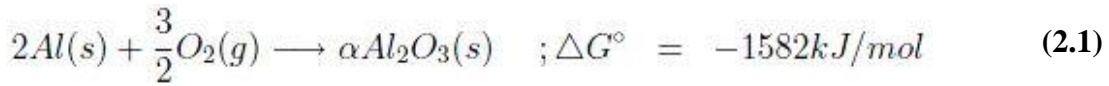
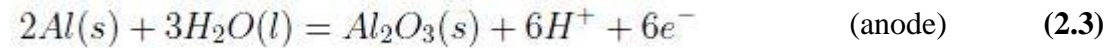


**Figure 2.10:** Elementary processes during pore growth (Bandyopadhyay, 2003)

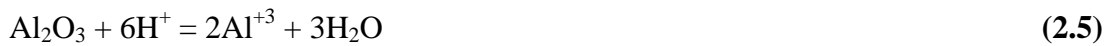
Thermodynamically, the spontaneous reaction forming the alumina layer is described by the large negative Gibb's free energy change below (Alpay, 2009):



During anodizing, the anode and the cathode reactions are:



The dissolution reaction of alumina is expressed as (Bandyopadhyay, 2003):



Kinetically, the current density that passes across the alumina layer can be expressed as the equation below:

$$j = j_a + j_c + j_e \quad (2.6)$$

In the equation,  $j_a$  is the anion contributing,  $j_c$  is the cation contributing and  $j_e$  is the electron contributing current density. Since aluminum oxide is an insulator, the electronic conductivity is very low. Therefore, ionic current density,  $j_i$ , which is the

sum of  $j_a$  and  $j_c$ , is crucial in charge transportation. In order to express the relationship between the electric field applied  $E$  and  $j_i$ , Guntherschultze-Betz equation is used:

$$j_i = j_0 \cdot \exp(\beta E) \quad (2.7)$$

$j_0$  and  $\beta$  terms in the equation are temperature and metal dependent terms and their value for aluminum oxide is around  $1 \times 10^{-16}$  to  $3 \times 10^{-2}$  mA/cm<sup>2</sup> and  $1 \times 10^{-7}$  to  $5.1 \times 10^{-6}$  cm/V.  $E$  on the other hand, varies from  $10^6$  to  $10^7$  V/cm.

According to the Guntherschultze-Betz equation, the ionic transport at the metal/oxide layer or at the oxide/electrode interface is the rate-limiting step; which is now generally accepted that oxides build up at both interfaces (Alpay, 2009).

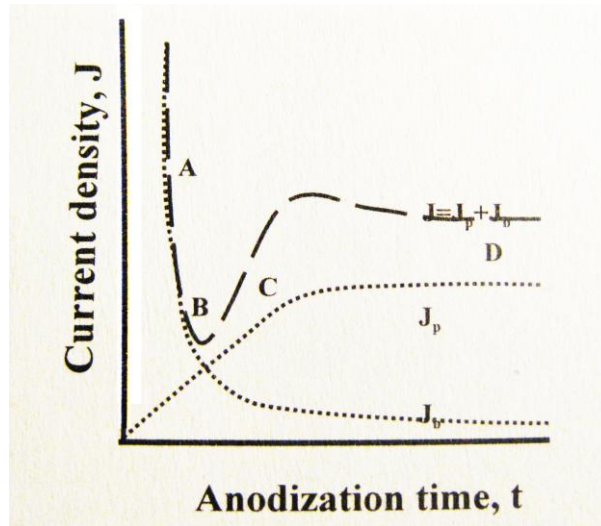


**Figure 2.11:** Current density as a function of time (Bandyopadhyay, 2003)

In figure 2.11,  $J_b$  stands for the current for the growth of the barrier layer and  $J_p$  is used for the current for the pore growth. The sum of  $J_b$  and  $J_p$  equals to the net current ( $J$ ) passing from the system. Mainly four phases can be observed during the anodizing. During the first few seconds of anodizing, the net current decreases until a minimum limit is observed. A zone is the region that an oxide layer is initially formed. Fine featured pores start to grow in the B zone and get enhanced in the C zone. The pores are stabilized in the D zone and the later gets thicker as the time for anodizing passes (Bandyopadhyay, 2003). Sulka and Stepniowski made experiments on different voltages and temperatures to investigate the net current behavior by time (2009). It can clearly be seen from figures 2.12 and 2.13 that, the voltage and

temperature have positive influence on the current density when it reaches the constant value.

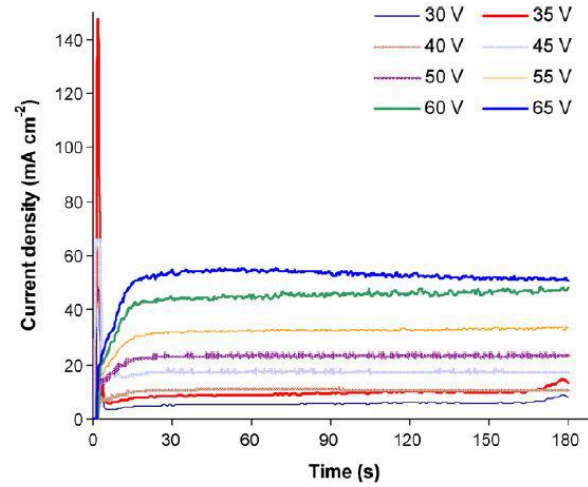


**Figure 2.12:** Current density vs. anodizing time by different voltages (Sulka,2009)

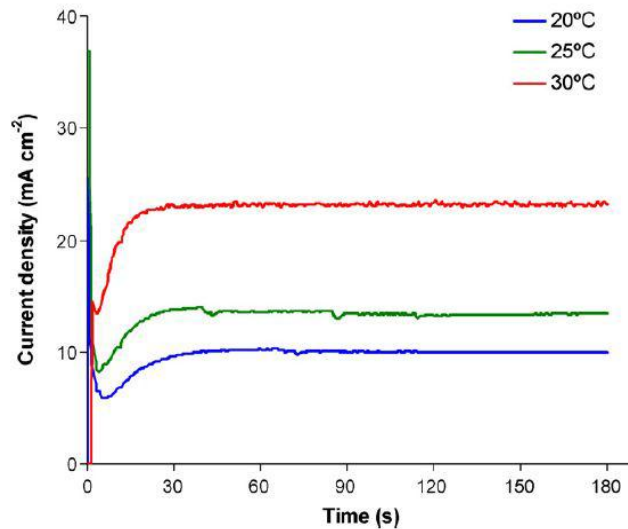


**Figure 2.13:** Current density vs. time by different temperatures (Sulka, 2009)

Anodizing can be completed in one step, as well as it can be performed in two steps in order to grow well organized pores. Masuda and Fukuda in their work in 1995, used two step anodizing and gathered more successful results compared to one step anodizing. They firstly anodized Al for five minutes in order to form texture on the surface and etched the alumina by 0.2M chromic and 0.4M phosphoric acid solution in 60°C for 5 minutes. Afterwards, another step of anodizing was followed for 12-18



hours in order to get ordered pore arrays. As a result, they managed to get rid of possible defects that is commonly observed in one step process.

## **2.5 Template –Assisted Synthesis Techniques Using Porous AAO**

After the anodizing process, the pores can be filled with the material that the nanowire will consist of. According to the literature obtained, there exist a few common techniques for filling AAO membranes:

- Pressure Injection
- Vapor Deposition
- Sol-gel Deposition
- Electrodeposition

### **2.5.1 Pressure Injection**

Pressure injection is a preferred method if highly crystalline nanowires are desired to be produced from materials with low melting points. It is based on injecting the liquid material with pressure, into the pores of the template. The template can be made of oxides that have high mechanical, thermal strength and chemical stability; which is crucial as the pressure and temperature rises during pressure injection. Until now, AAO and nano-channel glass materials have successfully been used as templates in order to produce metal nanowires like Bi, In, Sn and Al and semiconductor nanowires like Se, Te, GaSb and Bi<sub>2</sub>Te<sub>3</sub>. Metal oxide nanowires cannot be produced by this method due to their high melting points. It is possible to produce high crystalline nanowires with preferred orientations (Bhushan, 2004; Shankar, 2005).

It was also noted in the literature that, Huber et al. managed to produce metallic nanowires made of In, Sn, Al as well as semiconducting nanowires from Se, Te, GaSb, Bi<sub>2</sub>Te<sub>3</sub> (1994). In the method, the filling material and the template are placed in a thin-walled metal tube; which is sealed at one end. A vacuum system exists on the other side of the tube. The metal tube is first heated in an oven below the melting temperature of the filling material and vacuum dried for a couple of hours. Then the tube is cooled down to the room temperature, filled with a type of inert gas. After

being sealed, the temperature is risen above the melting temperature of the injected material as the pressure is increased step-by-step, so that the material is filled inside the tubular gaps in the template.

Washbur equation is used for calculating the pressure necessary for the injection, which is as given below:

$$d = -4\gamma\cos\theta/P \quad (2.5)$$

In the equation,  $d$  is the diameter of the pores of the template,  $\gamma$  is the surface tension of the liquid,  $\theta$  is the contact angle between the liquid and the template and finally  $P$  is the applied pressure (Bandyopadhyay, 2003).

### 2.5.2 Vapor Deposition

There are mainly two techniques that are employed: Physical Vapor Deposition (PVD) and Chemical Vapor Deposition (CVD). Small diameter nanowires ( $\leq 20\text{nm}$ ) can be produced by vapor deposition technique, which is a great advantage when it is compared to pressure injection.

In physical vapor deposition, before being filled in the pores of the template, the source material is heated to produce vapor and cooled down after contacting the pore surface. The process is controlled by temperature, pressure and carrier gas flow.

Bismuth (Bi) nanowires with the diameter of 7 nm can be deposited in AAO membranes with preferred crystal orientation. As for a semiconductor example produced by PVD method was reported on cadmium sulfide (CdS) nanowires which have important optoelectronic applications for laser light-emitting diodes and optical devices. According to the literature obtained, dried CdS powders were calcinated at in argon atmosphere and then deposited in the pores of AAO membrane with around 20nm in diameter. Metal oxide nanowires can also be produced. ZnO nanowires networks with the diameter around 100 nm can be produced by physical vapor deposition with a very good repeatability; which can be used for gas sensing and solar cells (Bhushan, 2004; Wu, 2002; Jimenez-Cadena et al, 2010).

Apart from PVD, Chemical Vapor Deposition can be used for compound materials composed of two or more reacting gases. The deposition is performed under high temperature conditions and specified gas atmosphere. For instance, ammonia ( $\text{NH}_3$ )

and gallium oxide ( $\text{Ga}_2\text{O}$ ) vapor can be used for single crystal GaN nanowire synthesis on AAO membranes. Si nanowire arrays were also reported to be produced by CVD on AAO. Silicane ( $\text{SiH}_4$ ) and hydrogen gases ( $\text{H}_2$ ) were used as reacting gases (Bhushan, 2004; Mengke, 2001).

### **2.5.3 Sol-gel Deposition**

Sol-gel processing is taken into account as another method for metal oxide nanowires of wide band gap n-type semiconductors, such as  $\text{TiO}_2$ , CdS, ZnO and  $\text{SiO}_2$ , since it is a powerful approach to prepare highly stoichiometric nanocrystalline materials. Sol-gel method is initially based on hydrolysis of a solution of precursor molecules; which can be either organic metal alkoxides in organic solvents or inorganic salts in aqueous media. A suspension of colloidal particles (sol) is produced and turns into a “gel” by the condensation of the sol. Finally, annealing can be done in order to obtain crystallized nanowires (Su, 2007; Shankar, 2005).

Zirconia nanowire arrays were produced by sol-gel method in the experiments of Xu (2003). Zirconyl chloride ( $\text{ZrOCl} \cdot 8\text{H}_2\text{O}$ ) was dissolved in absolute alcohol in order to obtain precursors at room temperature. After aging for 24 hours, the solution turned into a sol. AAO membrane was then soaked in the sol and dried. After being heat treated at  $600^\circ\text{C}$ , zirconia nanowires were produced around 200nm in diameter and  $50\mu\text{m}$  in length.

The sol may also be used for deposition by passing current from the system; which is then called electrophoretic method.  $\text{Fe}_2\text{O}_3$  nanowires were produced with this method by Lin and his colleagues (2003). Precursor was prepared by dissolving iron (III) nitrate in 2-methoxyethanol solution ( $\text{C}_6\text{H}_8\text{O}_2$ ) and then a platinum sheet was used as the anode, and an AAO with an Au substrate attached to a Cu foil was used as the cathode with the external potential difference of 5V. Annealing was done in order to crystallize  $\text{Fe}_2\text{O}_3$  nanowires with the diameter around 50 nm.

### **2.5.4 Electrochemical Deposition**

Electrochemical deposition, also known as electrodeposition, is a method based on diffusion of charged ions under an applied electric field, inside an electrolyte. The reduction and oxidation of charged ions takes place on surfaces, which are called

electrodes. The electrodeposition system is made of an anode, a cathode, an electrolyte and a power supply.

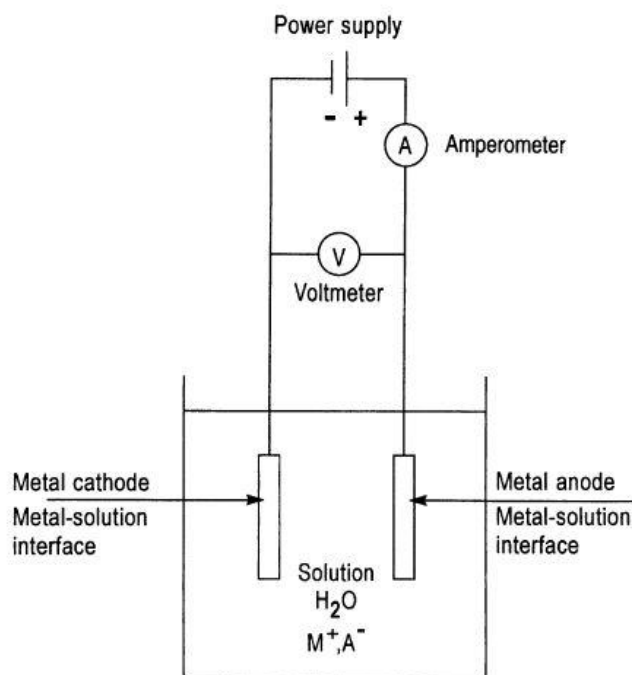


**Figure 2.14:** Representation of an electrodeposition system (Paunovic, 2006)

When an electric field is applied externally between two different electrodes, electrochemical reactions occur due to the flow from one electrode to the other. The electrode which is connected to the positive side of the power supply is called “anode”. Oxidation reactions occur on the surface anode. The negative electrode is called “cathode”, where the reduction of metallic ions take place which is also called deposition (figure 2.14). The conductive nanowire growth is a self-propagating process in electrodeposition. The electric field and the density of current lines between the tips of nanowires and the counter electrode becomes greater than the value between two electrodes once the little rods form. This happens due to the smaller distances between the nanowires and the electrodes. If the template pore size and thickness parameters are controlled, it is possible to control the morphology as well as the size of the deposited nanowires. The figure 2.15 shows the change of current versus time according to the deposition of nanowires inside the pores of the membrane used. The current during the deposition does not significantly change until the deposition is completed inside the pores (region I). The current then starts to increase right after the pores are filled (region II). Afterwards, the current increases until it reaches a plateau (region III) (Cao, 2008; Bhushan, 2004).

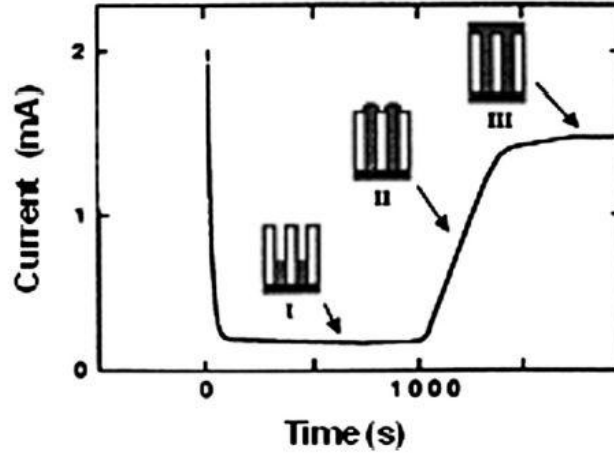


**Figure 2.15:** Current vs. time due the nanowire deposition inside the membrane (Cao, 2007)

The electrode potential is expressed by the Nernst equation given in equation 2.8.

$$E = E_0 + \frac{RT}{n_i F} \ln(a_i) \quad (2.8)$$

In the Nernst equation,  $E_0$  represents the standard electrode potential which is also equal to the potential difference between the electrode and the electrolyte.  $F$  is Faraday's constant,  $a_i$  is the activity of ions,  $R$  is gas constant and  $T$  is temperature. If the electrode potential is greater than the energy level of a vacant molecular orbital inside the electrolyte, the electrons transfer from the electrode to the solution. As a result of the movement, the electrolyte is reduced. In contrast, if the electrode potential is lower than the energy level of a vacant molecular orbital in the electrolyte, this time the electrons move from the electrolyte to the electrode, which oxidizes the electrolyte. These two phenomenons are shown in the figure 2.11a and 2.11b.

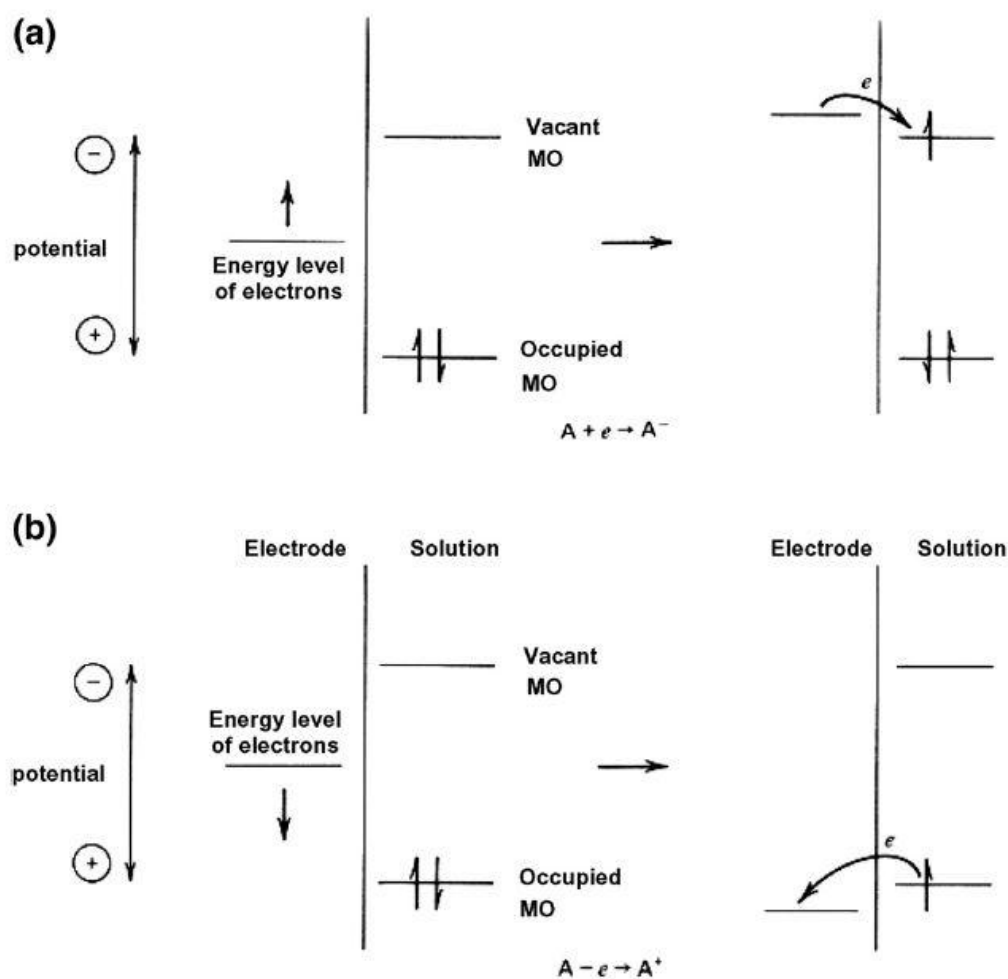


**Figure 2.16:** (a) reduction and (b) oxidation process in “A” solution (Cao, 2007)

The electrochemical deposition has been and still is being used widely throughout the years for growing thin films on conducting surfaces due to its economical and simple application techniques. Furthermore, the method is controllable and can be integrated for nanowire production by penetrating the nanowire materials inside the pores of the template used, which is used as the cathode of the system. The growth takes place closer to equilibrium than vacuum deposition techniques. The current might be selected as DC or either AC. According to the literature obtained, this method has successfully been used for metals like Bi, Co, Fe, Cu, Ni, Ag and Au; for metal oxides like  $\text{In}_2\text{O}_3$ ,  $\text{SnO}_2$  and  $\text{ZnO}$  for conducting polymers; superconductors like Pb; semiconductors like CdS and even superlattice nanowires with two metals such as Cu/Co. There are also a few examples of single crystalline nanowires obtained from  $\text{TiO}_2$  and CdTe. On the other hand, the method is not suitable for multicomponent oxide nanowires due to their different diffusivity and different ionic sizes. The template that is chosen for electrodeposition needs to be chemically stable

and deficiencies have a negative effect on the nanowire growth. (Bhushan, 2004; Shankar 2005).

The electrodeposition of an alloy depends on the codeposition of two or more than two metals. The ions of the depositing metals need to be present in the solution to form a cathodic film. The figure 2.17 shows that the current densities will be different at the fixed cathode potential. For instance, at the cathodic potential of  $V_2$ , will be deposited with the ratio of  $j_3/j_4$  respectively for the metals A and B (Paunovic, 2006).

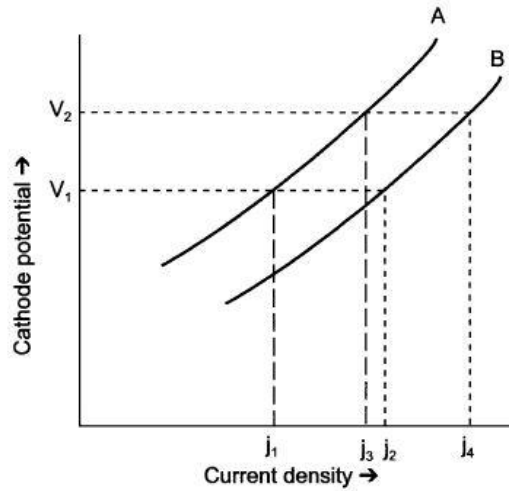


**Figure 2.17:** Polarization curves for the alloying elements (Paunovic, 2006)

During electrodeposition of alloys or metals, there are three main steps that should be taken into account:

- 1) Ionic Migration: The hydrated ions move to the cathodic region in the system due to the applied potential by diffusion and/or convection.
- 2) Electron Transfer: After the hydrated ions reach the cathodic surface, they enter to a double diffusion layer. In this part, the water molecules of the hydrated ions are separated; and then the metallic ion is neutralized and adsorbed.
- 3) Incorporation: The neutralized ions begins to deposit on the cathode surface and begins to grow the lattice of the alloy or the metal that is being deposited (Paunivoc, 2006).

It was reported in the literature that many metals, alloys and binary compounds can be electrodeposited by using AC electrodeposition. For instance Fe nanowires were successfully deposited on AAO in a  $\text{FeSO}_4$  with a Pt cathode by two different works of Xu and Haruyama (2000, 1998). The frequency range was selected between 100 and 1000 Hz. At every negative voltage cycle,  $\text{Fe}^{+2}$  ions supplied from  $\text{FeSO}_4$  migrated towards the alumina and were deposited in the pores of alumina.

For the case of DC electrodeposition method, the nonconducting barrier layer is a great problem and deposition cannot be achieved unless this barrier layer is removed. Figure 2.18 represents the structure of AAO on Al.

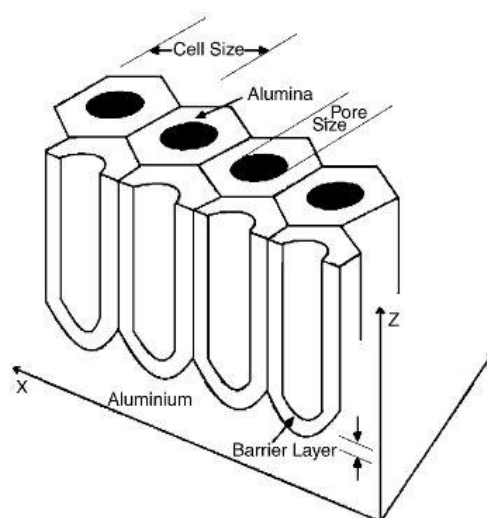


**Figure 2.18:** Schematic representation of AAO and its barrier layer (Saedi,2005)

According to the work of Cheng (2008), prior to Co-Ni deposition on AAO membranes, the surface of AAO was first obtained from two step anodization and then coated with Au in order to maintain conductance in the pores. Wu and his colleagues (2007) used sputtering method for making a thin Pt film prior to electrodeposition of Ni nanowires. The surface activation prior to electrodeposition is a very important step and various approaches can be gathered from the literature.

An organic layer can be used to cover the top of alumina pores after anodizing. Then the sample can be separated from the aluminum base by soaking in  $\text{HgCl}_2$ , so that the barrier layer is exposed in air. The barrier layer is then etched away in 5% phosphoric acid for a fixed amount of time. The organic layer is taken away and



porous alumina membrane is obtained. Finally, the bottom part can be coated with a conducting material and electrodeposition is achieved (Bandyopadhyay, 2003).

Electrochemical dissolution method is a promising method for modifying the pore bottoms of AAO membranes.. In this technique, at the end of the second step of the anodization, the applied voltage is lowered down to break the barrier layer at the bottom. Basically, as the voltage is decreased, the current is halved. When it reaches an almost steady state, it is halved again and vice versa as represented in figure 2.19. As a result, the bottom part of the barrier layer can be reduced by several tenths of nanometers (Santos, 2009; Jagminas, 2005).

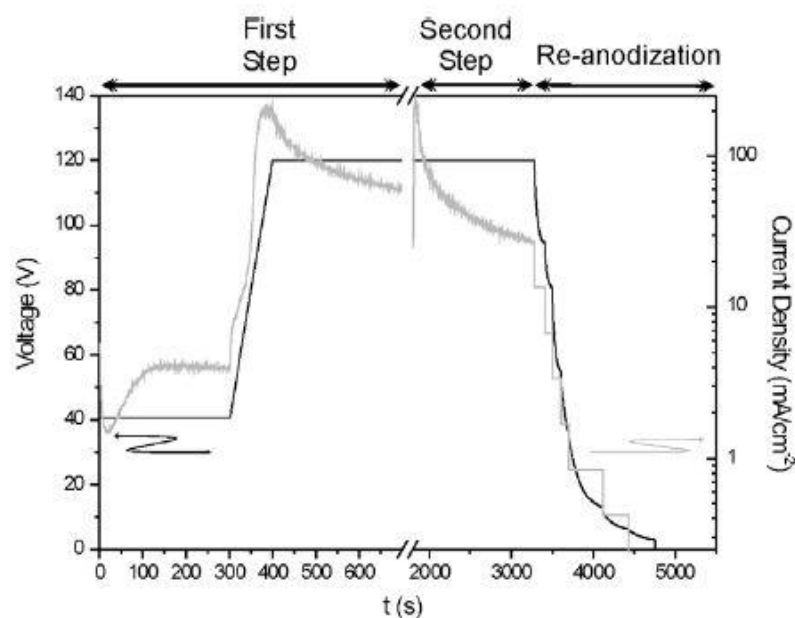


**Figure 2.19:** Typical current density–time and voltage–time curves by adding re-anodizing in the process (Santos, 2009)

Lillo and Losic suggested a controlled etching method for the removal of the barrier layer in 2008. As it can be seen from figure 2.15, the method is based on having two separate cells completing an electrolytic system and inserting the AAO layer between the contact area of the cells filled with 5% phosphoric acid.

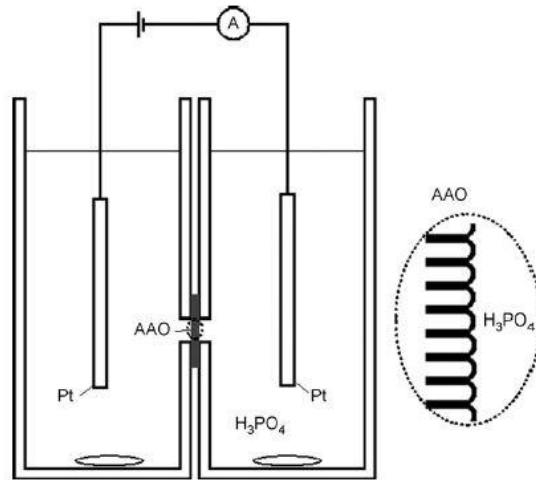


**Figure 2.20:** Schematic drawing of controlled dissolution system (Lillo, 2008)

The chemical etching by the phosphoric acid of the barrier layer was monitored from the current passing between the two cells and inside the AAO membrane (figure 2.21), as a small voltage of 1.5-2 V of potential difference was applied and both solutions were stirred.

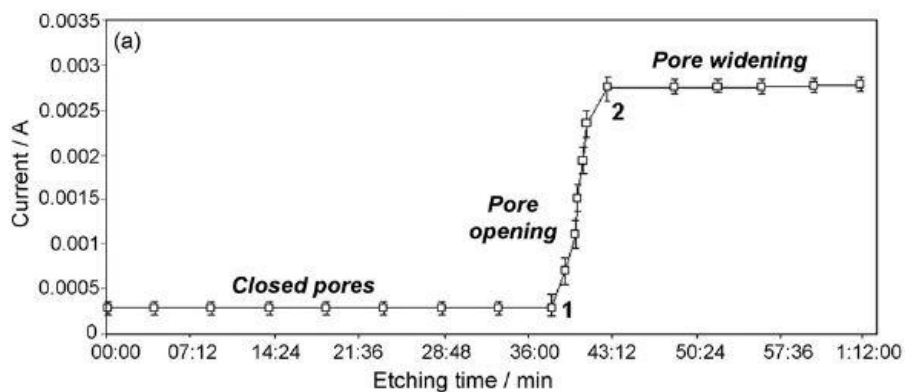
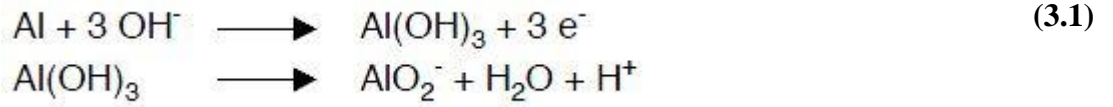


**Figure 2.21:** Pore opening curve (Lillo, 2008)

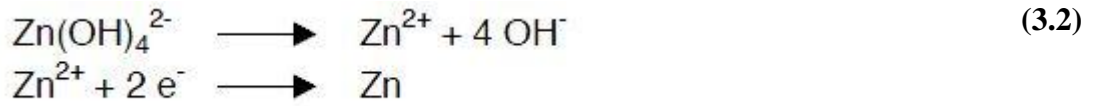
A significant single-step alternative for surface activation was suggested and patented by Urgan and Yeşil (2009) for the electrodeposition of free-standing nanowires. The method is based on utilizing zincating, which is widely used nowadays for Al surface activation prior to electrodeposition, by the removal of oxide layer on Al and the deposition of Zn on the surface. This thin conductive layer prevents reoxidation and maintains electrodeposition.

The zincate solution contains high concentration of NaOH. Therefore, when the zincate solution contacts with the barrier layer of AAO, the layer is etched away and two main events take place:

First oxidation reaction of Al occurs and aluminate ion ( $\text{AlO}_2^-$ ) is released



Afterwards, Zn is reduced and deposited on the surface after the barrier layer is etched.



In summary, this phenomenon is a way of material replacement or so called cementation of Al with Zn (Volk, 2004). This reaction enables the initiation of electrodeposition in the pores of AAO. It was asserted by Jin that, ultrasonic agitation during zincating increases the adhesion behavior as well the nucleation property of zinc compared to conventional method (2004). In the experimental part of the thesis work, the zincating process was conducted in an ultrasonic cleaner.



### **3. NI-W ALLOYS AND THEIR ELECTRODEPOSITION**

Ni-W alloys show a unique combination of properties due to their higher strength and hardness, improved tribological resistance, thermal properties such as high melting point, hot strength, oxidation resistance; as well as electrocatalytic and better corrosion properties when compared to elemental Ni. In industry, Ni-W alloys are used in barrier layers in copper metallization for ultra large scale integration devices (ULSI), microelectromechanical systems (MEMS), magnetic heads, bearings, resistors, electrocatalyzers for hydrogen evolution in alkaline solutions and an alternative for hard chromium coatings in aerospace. Ni-W systems are also preferred for their catalytic properties for desulfurization processes since most of the heavy chemical products such as oil refining, ferrous and non-ferrous metallurgy involve sulfurous compounds. (Krolikovski, 2009; Mitov, 2008).

#### **3.1 Mechanical and Corrosion Properties of Ni-W Alloys**

Tensile test is a conventional and reliable method for investigating the mechanical properties of materials. It gives out many information about elasticity, plasticity and fracture. Iwasaki, electrodeposited Ni-W alloys with the W at.% of 11.7 – 12.7 and carried on tensile tests with varied grain sizes depending on different current densities during deposition (2004). The current densities were 0.05, 0.007, 0.085 and 0.10 A/cm<sup>2</sup>. The grain sizes had a value between 8.1 to 8.6 nm according to the XRD analyses. The figure 3.1 shows the tensile strength values of the Ni-W alloys depending on the current densities.

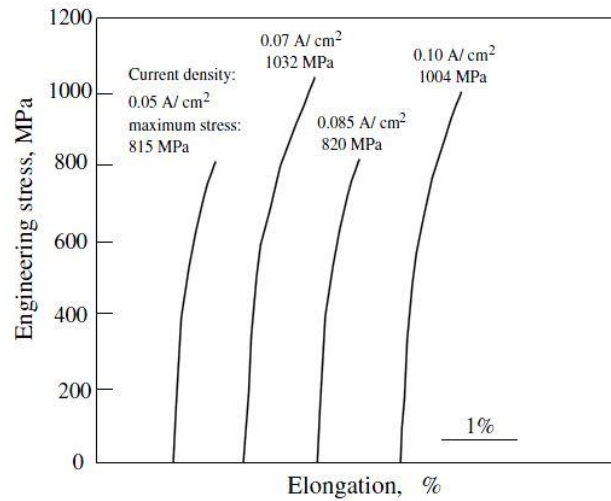


**Figure 3.1:** Tensile strength values vs. elongation curves (Iwasaki, 2010)

Hardness of coatings is also a very important parameter for the evaluation of mechanical properties of alloys. Sriraman and his colleagues investigated the hardness of electrodeposited Ni-W alloys with respect to the different W contents in the structure (2006). The figure 3.2 shows that the W content increased the hardness and showed a maximum value around at 9.33 at.% as the size of the crystallite decreases. After these values, a reverse Hall-Petch effect was observed.

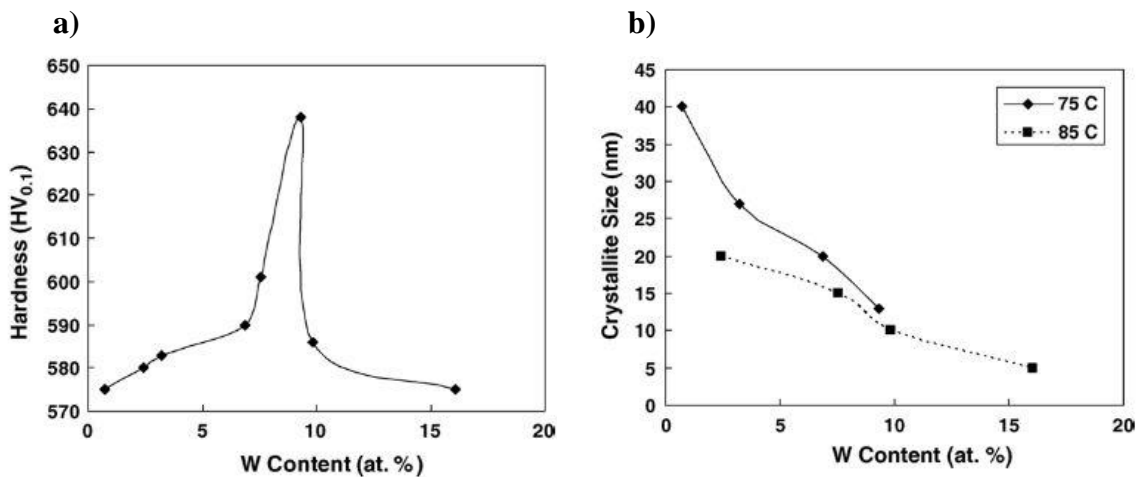


**Figure 3.2:** Effect of W to the hardness (a) and crystalline size in different temperatures (b)

The corrosion behavior of Ni-W alloys was investigated (Chianpariot, 2011). In the case of electrodeposited nanocrystalline Ni-W alloys, the number of prior experiments are very few. Chianpariot and his colleagues investigated the corrosion behavior of reverse-pulsed Ni-W electrodeposits in pH 3 and 10 3.5 wt.% NaCl

solutions. It was found out in the analyses that the corrosion rate increased as the grain size decreased in the case of alkaline environment. When the pH was 10, the grain size decreased from 63 nm to 39 nm.  $E_{\text{corr}}$  increased from -0.186 to -0.137 V versus standard calomel electrode (SCE) and  $i_{\text{corr}}$  decreased from 3.10 to 0.143  $\mu\text{A}/\text{cm}^2$  respectively. The potentiodynamic curves can be seen in figure 3.3. “mc nickel” in the figure stands for zero W content. According to the figure no apparent passivation behavior occurred at 5 wt.% W. The passivation behavior becomes more noticeable as the W content increases and disappears again in Ni-22W which corresponds to 5 nm grain size.

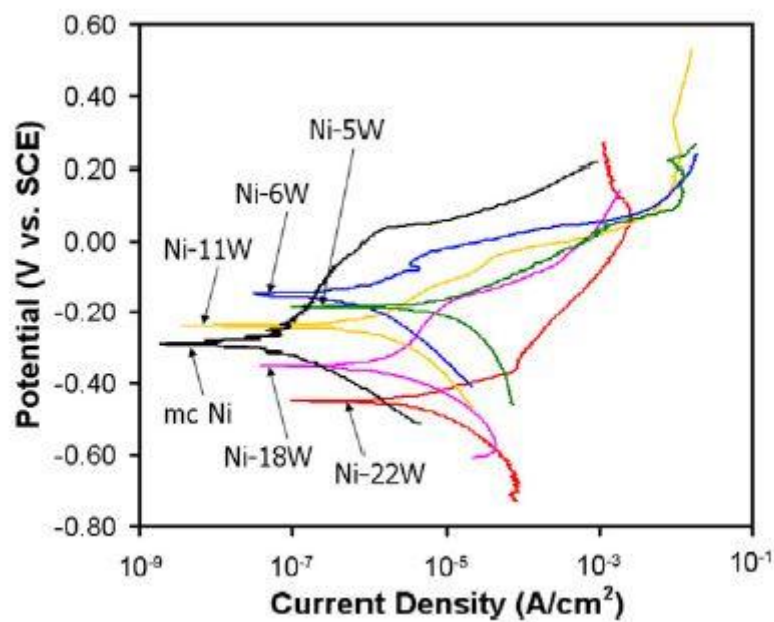


**Figure 3.3:** Potentiodynamic curves in 3.5 wt.% NaCl solution at pH 10  
(Chianpariot, 2011)

For the case of pH=3 in a 3.5 wt.% NaCl solution (figure 3.4), the pure electroplated Ni deposit does not show a passivation behavior. The  $i_{\text{corr}}$  is 3.35  $\mu\text{A}/\text{cm}^2$  and  $E_{\text{corr}}$  is 0.172 V vs SCE. It was also noted that mc-Ni showed pitting corrosion whereas the other specimens are corroded uniformly. The potentiodynamic curves can be seen in figure 3.3 for pH=3 in a 3.5 wt.% NaCl solution.

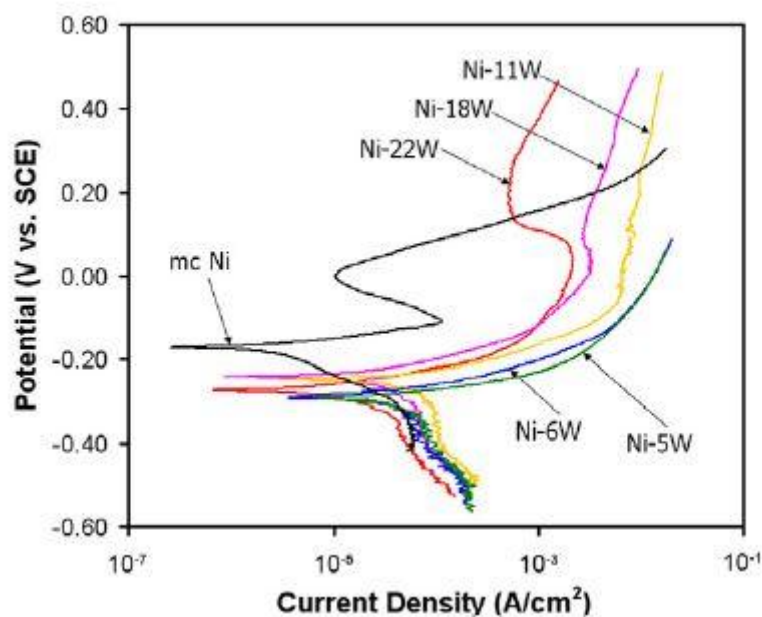


**Figure 3.4:** Potentiodynamic curves in 3.5 wt.% NaCl solution at pH 3 (Chianpariot, 2011)

The study of Chianpariot demonstrated that Ni-W alloys with grain sizes ranging from 5 to 63 nm exhibit higher corrosion rates in acidic media than alkaline media (2011). The corrosion rate of nanocrystalline Ni-W generally increases with the decreased grain size when pH is elevated. This is due to the increase in the grain boundary volume and its control mechanism of  $i_{\text{corr}}$ . On the other hand, in acidic environment, the corrosion rate of nanocrystalline Ni-W decreases with the decreased grain size. The higher W content is contributed to a stronger film, therefore it is the main factor for controlling the  $i_{\text{corr}}$ .

Electrocatalytic properties are one of the most investigated and important properties. Ni and Ni alloys are known as good electrocatalysts. It was asserted that the formation of intermetallics of transition elements that have half filled or partially filled d orbitals such as Mo, W, V with transition metals that have internally paired d-electrons such as Ni, Pd, Pt, Co etc. show a different bond strength, which increases the stability. This property makes Ni-W alloys a suitable candidate for hydrogen evolution reaction (HER) experiments. Hukovic and his colleagues made a research about the electrocatalytic properties of nanocrystalline Ni-W coatings (2006). Binary Ni-W alloy coatings with the W content ranging from 5-25 at.% were deposited by DC magnetron sputtering. The hydrogen evolution reaction test was conducted in an alkaline electrolyte. For comparison, another film of pure nickel



was deposited with the grain size of 10 nm. The obtained results clearly showed that, compared to Ni, alloying Ni with W increased the electrocatalytic activity and the HER. 10 at.% W showed the highest electrocatalytic activity.

Mitov and his colleagues examined the catalytic properties for desulfurization by Ni-W electrodeposits (2008). The hazardous effect of sulfurous compounds and the new environmental regulations makes hydrodesulfurization studies a must and new technologies are being developed for this issue. The results obtained showed that sulfide ions were successfully oxidized to sulfur by the catalytic effect of Ni-W electrodeposits.

The effect of heat treating on the mechanical properties of Ni-W alloys was investigated by Yamasaki (2000). Heat treating significantly increased the hardness of the alloys. On the other hand, increasing in deposition current also increased the W content in the deposit and decreased the grain size which is expressed in the table 3.1.

**Table 3.1:** Average grain sizes and Vickers microhardness values after electrodeposition in 348°K and annealing in 723°K (Yamasaki, 2000)

Current density (A/cm <sup>2</sup> )	W content (at. %)	Grain size (nm), as-deposited	HV, as-deposited	Grain size (nm), 723K-24 h	HV, 723K-24 h
0.05	17.7	6.8 (7.0)*	558	9.5	919
0.10	20.7	4.7 (3.0)*	635	9.0 (10)*	962
0.15	19.3	4.7	678	8.9	992
0.20	22.5	2.5 (Am.)*	685	8.2	997

( )\* : TEM observations

### 3.2 Electrodeposition of Ni-W Alloys

It is known that electrodeposition is a feasible method for producing Ni-W alloys due to their ease of control and economical use; which can be used for fabricating coatings as well as bulk products tungsten itself cannot normally be electrodeposited from an aqueous solution of sodium tungstate (Na<sub>2</sub>WO<sub>4</sub>) or other dissolved components in aqueous media containing tungsten unless it is used as a codeposition element with a suitable Ni compound. Nickel sulfate (NiSO<sub>4</sub>) is generally used as the main Ni source, which is used with Na<sub>2</sub>WO<sub>4</sub> the electrodeposition of Ni-W alloys. Likewise, Mo and Re are also elements that have the same behavior as W and need other elements like Ni, Co or Fe for codeposition (Sriraman, 2006 ; Eliaz, 2005).

From the Ni-W phase diagram given in figure 3.5, Ni-W phases are crystalline until 22-23 W at.% content and between 12-13 W at.% and 18-19 W at.%,  $\text{Ni}_4\text{W}$  intermetallic compound can be seen with the Ni-W phase in the structure.

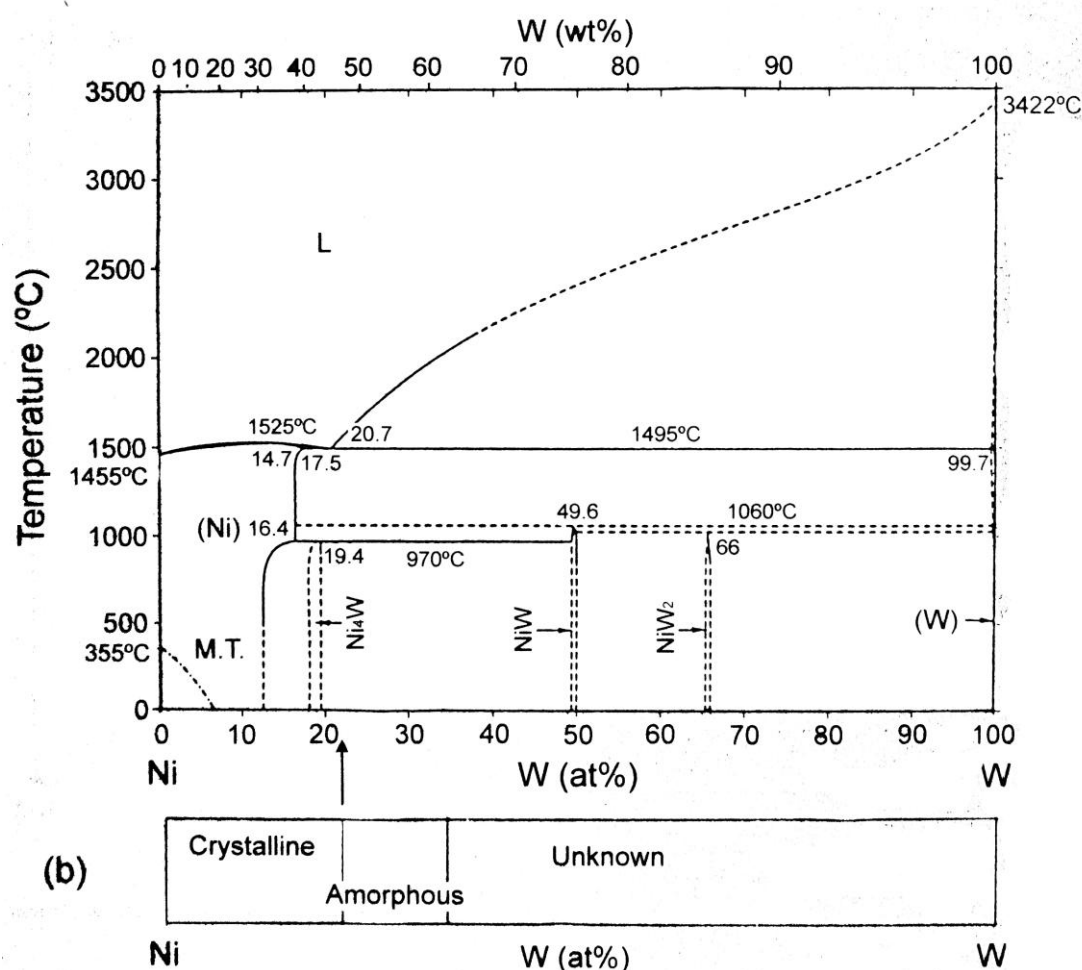


**Figure 3.5:** Ni-W phase diagram (Watanabe, 2004)

Juskenas and his colleagues investigated the influence of W content in electrodeposited Ni-W fcc crystal structure (2009). Different pH levels and heat treatment conditions were analyzed. Between the range of pH 4-7, the W at.% content in the electrodeposited Ni-W fcc structure ranged from 14 to 18 respectively.

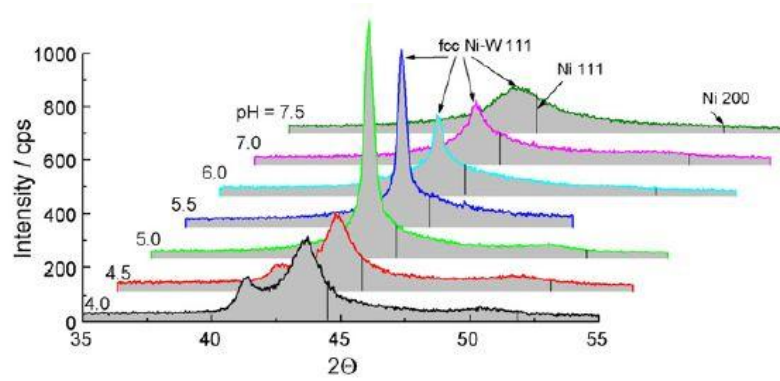


**Figure 3.6:** XRD patterns obtained from electrodeposited Ni-W alloys in different pH values (Juskenas, 2009)

Figure 3.6 shows the behavior of XRD patterns depending on different pH values. The patterns show  $\gamma$  phase peaks of 111 with different values of  $2\theta_{\max}$ . The obtained patterns show that the W content in the electrodeposited Ni-W  $\gamma$  phase crystallite size is affected by pH. At pH= 4 and 4.5, an extra peak of  $\text{NiWO}_4$  was observed at  $2\theta = 41.4^\circ$ .

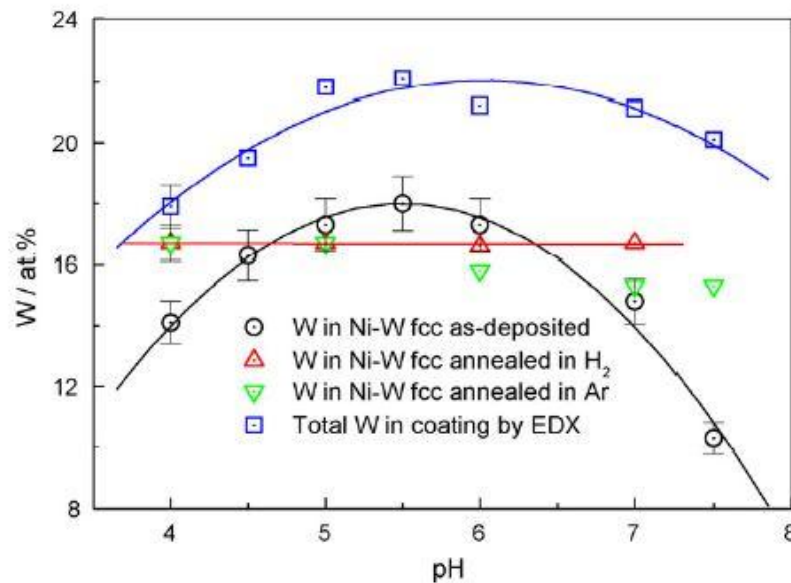


**Figure 3.7:** The total W quantity in the Ni-W alloy and W in Ni-W fcc phase as a function of pH (Juskenas, 2009)

Ni-W coatings containing up to 22 W at.% between the range of pH 4-7 can be obtained by electrodeposition according to figure 3.7. It can be seen that after annealing, the W content in the solid solution is nearly independent from pH and higher than the maximum solubility of W in Ni which is around 12-13.5 at.% (Juskenas, 2009).

Yamasaki, in his experiments, investigated amount of W content in the Ni-W alloy according to the varied current densities and their effects on crystallinity (2001). The figure 3.8 shows that increasing the current density of Ni-W electrodeposition has a positive affect on W at.% content in the alloy. It is also obvious from the XRD patterns that, increased W content in the Ni-W alloy decreases the crystallinity which is apperent from the width of the peaks with elevated W contents.

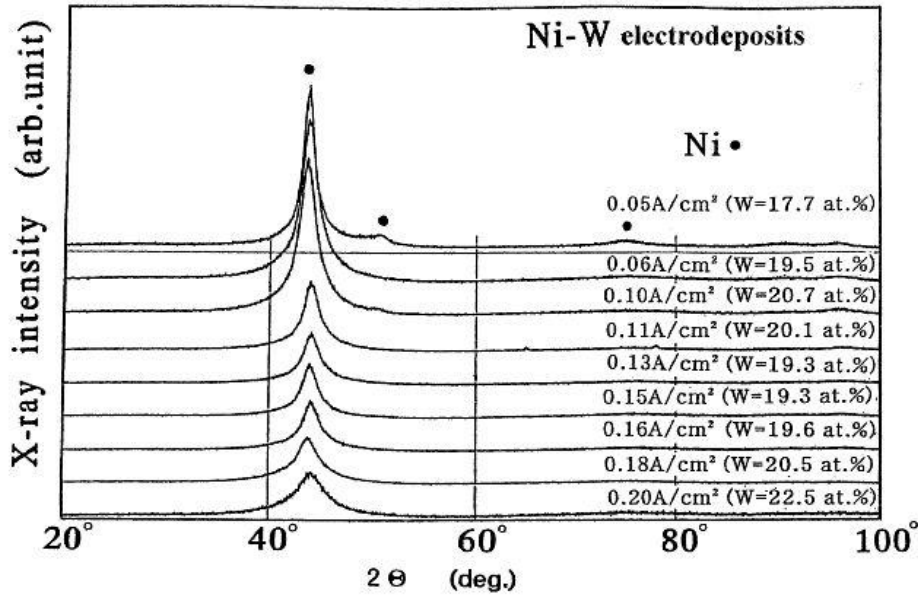
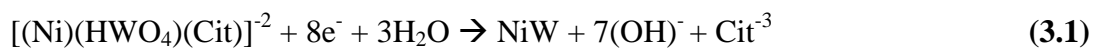


**Figure 3.8:** XRD patterns of electrodeposited Ni-W alloys for various current densities (Yamasaki, 2001)

Typical baths that are used for Ni-W alloys contain mainly three elements: A source for Ni and W, and a complexing agent. Nickel sulphate ( $\text{NiSO}_4$ ) is used as the Ni source and sodium tungstate ( $\text{NaWO}_4$ ) is used for W. Organic acids such as citric, tartaric, malic, gluconic, saccharic and hydroxyl acetic acids are added to improve the Faradaic efficiency and the metallic ion solubility. It was asserted that when citrate ( $\text{C}_6\text{H}_5\text{O}_7$ )<sup>-2</sup> is used as a ligand, which is the conjugate base of citric acid ( $\text{C}_6\text{H}_8\text{O}_2$ ), increases the W content to 50 at.% (76 wt.%). The precursor for Ni-W deposition is a mixed complex which is formed in the reaction given in the equation 3.1 (Metzler, 2003; Eliaz, 2005).



The Faradaic efficiency ( $\eta_F$ ) is the term used for the contribution of charges in the system to the electrochemical reaction and is calculated by the ratio of the actual coulombs obtained to the theoretical amount of electrons that can potentially be used in the system (Eliaz, 2005) . It is given in the equation 3.2 given below.

$$FE = \frac{w}{It} \sum \frac{c_i n_i F}{BM_i} \times 100 \quad (3.2)$$

In the Faradaic efficiency equation,  $w$  stands for the measured weight of the deposit (g),  $I$  is used for the current passing from the system (A),  $t$  is used for time (sec),  $c_i$  is used for the weight fraction of the depositing element in the binary alloy (which in this case is nickel or tungsten),  $n_i$  is the number of moving electrons used in the reduction in each mole (2 for Ni and 6 for W),  $M_i$  is the weight of the element per mole (g/mol),  $F$  is the Faraday constant (96485.3 C/mol) and finally  $B$  is a conversion factor (3600 C.A<sup>-1</sup>.h<sup>-1</sup>). It is also common to add ammonia (NH<sub>3</sub>) to the Ni-W electrolytes in order to increase the Faradaic efficiency. The pH is arranged by sulfuric acid (H<sub>2</sub>SO<sub>4</sub>) and sodium hydroxide (NaOH). These baths are typically used at temperatures of 50 –80°C (Eliaz, 2005).

Various parameters were examined on the codeposition of W in the presence of Ni. The concentration of WO<sub>4</sub><sup>-2</sup> was studied by Metzler (2006). In the experiments, the concentration of WO<sub>4</sub><sup>-2</sup> was kept less than the concentration of citrate. It was shown that the ratio of WO<sub>4</sub><sup>-2</sup> to Ni<sup>+2</sup> in the solution is not simply related to the W at.% content in the deposited alloy, but more complex. During the experiments, the Ni<sup>+2</sup> concentration was kept constant to 0.1 M. When the concentration of WO<sub>4</sub><sup>-2</sup> (0.3M) was around three times the concentration of Ni<sup>+2</sup>, Ni made a complex of [(Ni)(Cit)<sub>2</sub>]<sup>-4</sup> and this complex slowed down the deposition of Ni. Increasing the WO<sub>4</sub><sup>-2</sup> concentration increased the partial current for W deposition as well as of Ni. At 0.5 M, there was not enough citrate to make a complex of [(Ni)(Cit)]<sup>-4</sup>, but [(Ni)(Cit)<sub>4</sub>]<sup>-</sup>. Ni deposited more easily in this complex when compared to [(Ni)(Cit)<sub>2</sub>]<sup>-4</sup> which apparently increased the Ni amount in the deposit. On the other hand it was observed that changing the concentration of citrate increased the Faradaic efficiency.

The concentration change of  $\text{Ni}^{+2}$  was also investigated in a system consisting of 0.4 M tungstate and 0.6 citrate. The  $\text{Ni}^{+2}$  concentration ranged from 0.01M to 0.1M and as it increased, the partial current density of  $\text{WO}_4^{-2}$  increased with the partial current density of  $\text{Ni}^{+2}$  (Metzler, 2006).

Increasing the temperature directly affects the Faradaic efficiency. It was calculated that the FE had a value 27% at room temperature and 71% at 60°C. Also at 10°C, Faradaic effect was 11%. Therefore increasing the deposition temperature also increases the Faradaic effect (Metzler, 2006). It was asserted in the article of Sriraman that high temperature caused amorphous Ni-W deposits and the tungsten amount in the deposit stayed the same as the operating temperature ranged from 10°C to 60°C (2006). Similar statements about the deposition behavior of Ni-W alloys in varied deposition temperatures are observed also in the work of Eliaz (2005).

The effect of pH is also a crucial element. As it can be seen from the figure 3.3, the pH has a direct effect on the W content in the structure (Juskenas, 2009). A similar trend was also observed by Metzler. If there is ammonia inside the electrolyte, both Faradaic efficiency and the partial current of Ni increases with the increasing pH. On the other hand, in the absence of ammonia, FE and partial current density of Ni decreases as the pH increases. The W content of the deposits were not affected by the presence of ammonia (2006).

#### 4. EXPERIMENTAL PROCEDURE

The experimental studies that were conducted for producing Ni-W nanowires by using AAO templates are schematically outlined in figure 4.1. The AAO templates were produced by anodization in oxalic acid. After pore bottom activation with a special process developed in our group, the Ni-W nanowires were deposited by DC electrodeposition into the pores of AAO templates.

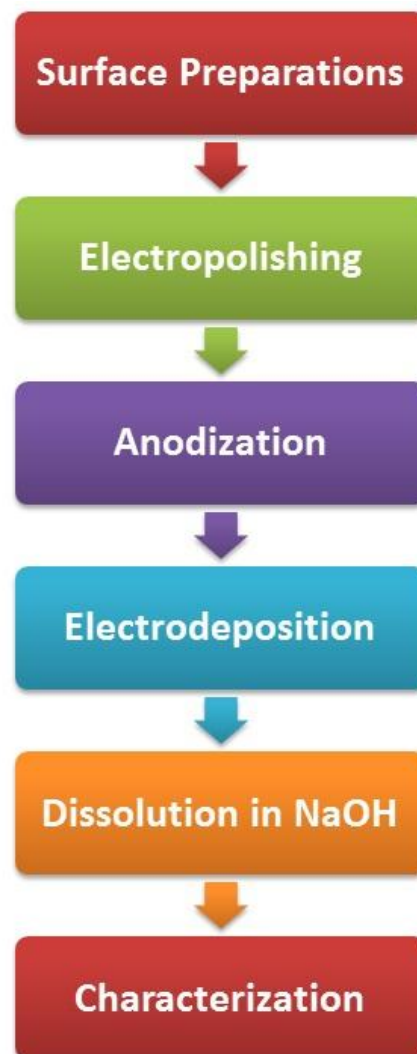


**Figure 4.1:** Steps of the experimental procedures

#### 4.1 Surface Preparations

Pure aluminum plates with the thickness of 0.5 mm were cut in the dimensions of 2x4 cm. Annealing was performed in 500°C for 4 hours, and the grain sizes were increased in order to obtain better surface quality prior to anodizing. The Al plates were subjected to standard alkaline etching and desmutting procedure in 10 wt% NaOH solution for five seconds in 55°C for etching and in 10% HNO<sub>3</sub> solution for five minutes at room temperature for desmutting.

#### 4.2 Electropolishing

The surface of Al sheets were electropolished in order to obtain smooth AAO surfaces after anodization. A commercial, Cr free solution based on phosphoric – sulphuric acid mixture was used for this step (Politoksal EB-35 from Politeknik Metal San. ve Tic. A.Ş.). The parameters used for electropolishing are given below in table 4.1.

**Table 4.1:** Operating conditions of electropolishing solution

<b>Temperature</b>	<b>65-70°C</b>
<b>Operation Time</b>	<b>1-12 min.</b>
<b>Voltage</b>	<b>17-25 V</b>
<b>Current Density</b>	<b>10 A/dm<sup>2</sup></b>

#### 4.3 Anodizing

Anodizing step is one of the most important steps prior to electrodeposition. The final properties of AAO layer deposited on Al depends on the surface quality of Al and the anodization conditions.

Experiments were conducted in a water jacketed glass container, attached to a cryostat (mgw Lauda RM6-RMT) using 0.3 M oxalic acid solution. During the experiments, the solution was continuously stirred with the help of magnetic stirrer. 316 stainless steel sheets were used as cathode. A regulated DC power supply (Sorensen DCS150-20E) capable of supplying max. 150 V and 20 A was used during anodization experiments. . The area ratio of aluminum plate to the stainless steel was



set as 0.2. During anodizing, agitation speed was kept constant to 800 rpm, in order to maintain temperature homogeneity and oxygen feeding.



**Figure 4.2:** Anodizing system

Both single and two step anodization was performed using electropolished and mechanically polished pure aluminum substrates to show the effects of surface preparation, two step anodization as well as anodization voltage and temperature parameters on the morphology of the AAO templates. In two step anodization anodic oxide formed in the first step was etched by using 6% wt.  $\text{H}_3\text{PO}_4$  and 1.8% wt.  $\text{H}_2\text{CrO}_4$  solution at  $60^\circ\text{C}$  for one hour.

An additional experiment (electrochemical dissociation) was conducted for thinning of the barrier layer that was formed at the bottom of the two step anodized aluminum. In these experiments the anodization voltage was lowered for 70 to 15 V with a rate of 0.1 V/s, thereon the anodization continued for 30 more minutes. The parameters used for anodization are summarized in table 4.2.

**Table 4.2:** Anodizing parameters

Temperature (°C)	First Step	Second Step	Electrochemical Dissociation	Zincating	Purpose
10	70V/2.5min	-	-	-	Effect of electropolishing on the surface
5	30V/1h	30V/1h	-	-	Pore size and layer thickness
25	30V/1h	30V/1h	-	-	Pore size and layer thickness
5	50V/20min	50V/20min	-	-	Pore size and layer thickness
25	50V/20min	50V/20min	-	-	Pore size and layer thickness
5	70V/5min	70V/5min	-	-	Pore size and layer thickness
25	70V/5min	70V/5min	-	-	Pore size and layer thickness
25 (1 <sup>st</sup> step) & 5 (2 <sup>nd</sup> step)	40V/1h	70V/5min	15V/30min		Barrier layer investigation and electrodeposition
25 (1 <sup>st</sup> step) & 5 (2 <sup>nd</sup> step)	40V/1h	70V/5min	15V/30min	25 sec (30-35 °C)	Barrier layer investigation and electrodeposition

Performing the experiments at different voltages and temperatures enabled us to calculate the AAO growth rate for further optimization. After determining the growth rate, in order to obtain hexagonal, ordered anodized structures, different methods were investigated by applying different voltages and temperatures in both steps of anodizing.

#### **4.4 Pore Bottom Activation**

It is known that inside the porous structure of AAO there exists a barrier layer at the bottom which is a thin, insulating layer. The bottom part of the pores needs to supply charge transfer for electrodeposition of nanowires on AAO membranes. Therefore, the combination of electrochemical dissolution was applied and afterwards the bottom of the pores were subjected to zincating for opening the pore bottoms and also make them DC electrodepositable with the help of very thin zinc layer deposited on the opened pore bottoms. .

In the experiments, electrochemical dissolution was conducted right after the second step of anodization by reducing the applied voltage with the rate of 0.1 V/sec. to 15V and anodizing was continued for more 30 minutes. A zincate solution containing 2 g/l  $\text{FeCl}_3$ , 50g/l  $\text{C}_4\text{H}_4\text{KNaO}_6$ , 120 g/l  $\text{NaOH}$ , 20 g/l  $\text{ZnO}$ , 1 g/l  $\text{NaNO}_3$  was used after electrochemical dissolution. The method relies on the principles described by Urgan and Yeşil (2009) and the zincating parameters that were optimized in previous studies (Alkan,2009; Karahasanoglu, 2009) conducted within “Surface Technologies Group” laboratories. Anodized and rinsed AAO templates were dipped in previously heated zincate solution in ultrasonic cleaner. The temperature of the solution was between 30-35°C, and duration was 25 seconds.

#### **4.5 Electrodeposition of Ni-W Nanowires**

Electrodeposition was conducted in a solution that contained 0.1 M  $\text{NiSO}_4 \cdot 6\text{H}_2\text{O}$ , 0.3M  $\text{Na}_2\text{WO}_4 \cdot 2\text{H}_2\text{O}$  and 0.28M  $\text{C}_6\text{H}_8\text{O}_7 \cdot 2\text{H}_2\text{O}$  which was prepared in 500ml solution (table 4.3) the pH of the solution was set to 3-3.3.

In order to check the possibility of electrodeposition of Ni-W alloy on aluminum, aluminum surface is zincated for 10 s and then subjected to deposition process using

a current density of 4 A/dm<sup>2</sup>. The temperature of the solution was set to 60°C and kept constant within +/- 2 °C during deposition.

**Table 4.3:** Chemical composition of the Ni-W electrolyte

Chemical	mol/l	Function
NiSO <sub>4</sub> ·6H <sub>2</sub> O	0.1	Ni source
Na <sub>2</sub> WO <sub>4</sub> ·2H <sub>2</sub> O	0.3	W source
C <sub>6</sub> H <sub>8</sub> O <sub>7</sub> ·2H <sub>2</sub> O	0.28	Complexing agent

After successful achievement of electrodeposition on zincated aluminum surfaces, pore filling experiments has been started aiming to investigate the role of deposition current density on the structure and morphology of nanowires.

Pore bottom activated (zincated) AAO template was used as cathode and a Pt mesh was used as anode. The distance between the anode and the cathode was set to 3 cm and the deposition was conducted under current control. Current values ranged from 1.25 A/dm<sup>2</sup> to 2.5 A/dm<sup>2</sup> for apparent surface area of 16 cm<sup>2</sup>.

After the deposition process, the specimen was thickened around 45 minutes by nickel electrodeposition solution Watts bath, in order to protect the Ni-W layer and for the ease of holding. The composition of the Watts solution is given in table 4.4. The electrodeposition process was conducted at 55°C at 6A/dm<sup>2</sup> for 45 minutes until the thickness was sufficient for the ease of holding the samples after dissolution of Al.

**Table 4.4:** Chemical composition of Watts solution

Chemical	Concentration
NiSO <sub>4</sub> ·6H <sub>2</sub> O	0.9 mol/l
NiCl <sub>2</sub> ·6H <sub>2</sub> O	0.12 mol/l
H <sub>3</sub> BO <sub>3</sub>	0.48 g/l

## **4.6 Dissolution of AAO Templates**

The final product that contained Ni-W nanowires was left in 10 wt% NaOH solution at 55°C until Al and AAO was etched away and the nanowires were obtained. The specimens were then characterized.

## **4.7 Characterization of Ni-W Nanowires**

### **4.7.1 XRD Analyses**

The nanowires obtained were analyzed by Philips PW-3710 XRD analyzer with the X-ray radiation of Cu- $\alpha$  (40kV- 40mA) and the entrance angle of 1° in order to prevent the possible peaks from the base plate. Scanning was conducted within the range of  $2\theta = 10-90^\circ$ . The patterns were then compared to the data in X'pert High Score Software.

### **4.7.2 FEG-SEM and EDS Analyses**

The FEG-SEM images were obtained by Jeol™ JSM-7000F from the top and the cross sections of the specimens to investigate their morphology. EDS analyses were also performed for determining atomic composition of the nanowires.

### **4.7.3 Polarization Curve Analyses**

Polarization curves were obtained by Princeton Applied Research Potentiostat/Galvanostat 263A. The experiments were conducted in a 1M NaOH solution at 25°C and was deaerated by purging with N<sub>2</sub> for 30 minutes prior to experiments. The experimental set-up and parameters used are similar to the experimental procedure described by Hukovic et al. (Hukovic, 2006). N<sub>2</sub> was passed over the solution to keep the system deaerated. A saturated Ag/AgCl reference electrode was used in the experiments. Nickel coated Al plate and Ni-W coated Al plate was also tested in order to compare with the data obtained from Ni-W nanowires, providing the same apparent surface area of 4cm<sup>2</sup> for all samples.



## 5. RESULTS AND DISCUSSIONS

### 5.1 Optimization of Anodizing parameters

#### 5.1.1 Effect of Surface Finish on the Morphology of AAO

The effect of surface finish on the morphology of AAO were investigated by using a mechanically and electro-polished pure aluminum samples that were subjected to anodizing under identical conditions. It can clearly be seen from figure 5.1 and 5.2 that electropolishing is very effective for obtaining smoother AAO surfaces. Both samples had pore diameters around 30 nm after anodizing at 70V for 2.5 minutes at 10 °C. These two specimens were subjected to single step anodization.

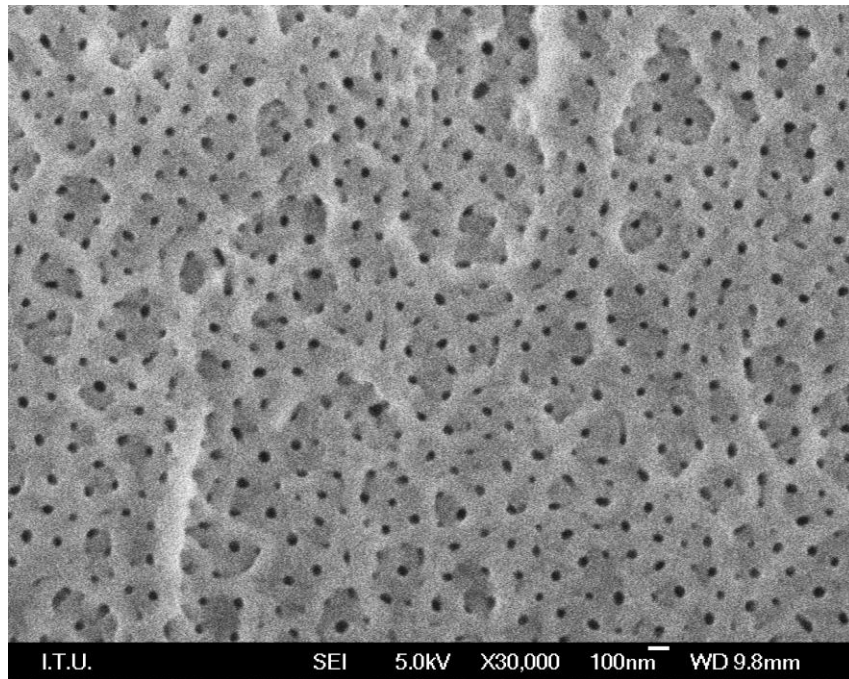


**Figure 5.1:** FEG-SEM image of AAO surface without electropolishing

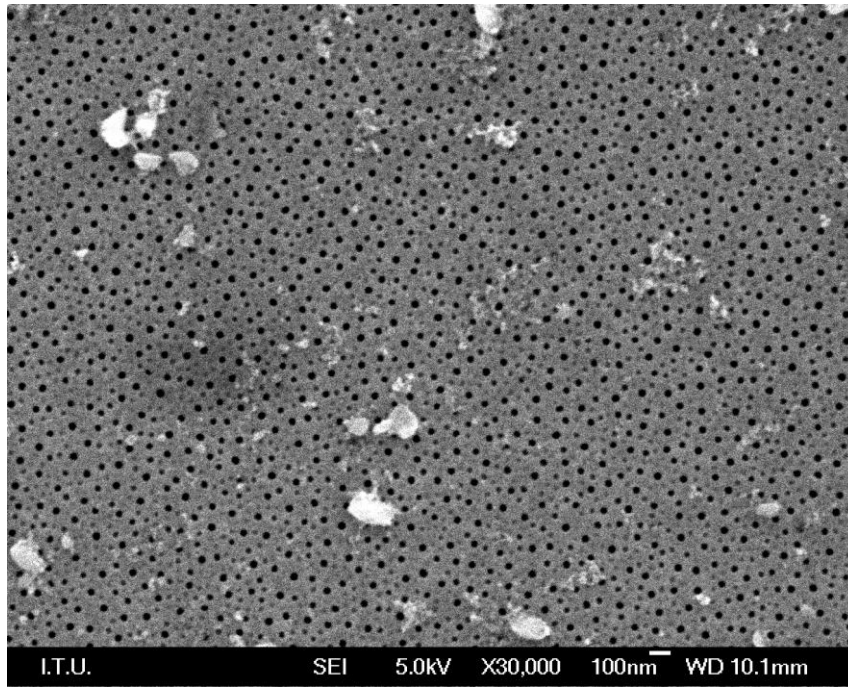


**Figure 5.2:** FEG-SEM image of AAO surface produced on electropolished aluminum

Electropolishing process drastically improved the final surface smoothness of the AAO layer. On the other hand, the pore distribution was not homogenous in both samples obtained. In order to increase the regularity of the pores and their distribution it was decided to conduct further anodization experiments with two step anodization process.

### 5.1.2 Pore Size and Thickness of AAO

Two step anodizing was performed at different anodization voltages (30V, 50V and 70V) and temperatures (5°C and 25°C). Between the two steps, anodized aluminum was etched with 6% wt.  $\text{H}_3\text{PO}_4$  and 1.8% wt.  $\text{H}_2\text{CrO}_4$  solution at 60°C for one hour. This process maintained a well ordered hexagonal Al base for a better distribution of pores inside the AAO layer in the second step of the anodization (Figure 5.3). According to the FEG-SEM images obtained, increasing the applied voltage also increases the pore size. Figure 5.4 shows the pore diameters of AAO templates obtained at 5°C.



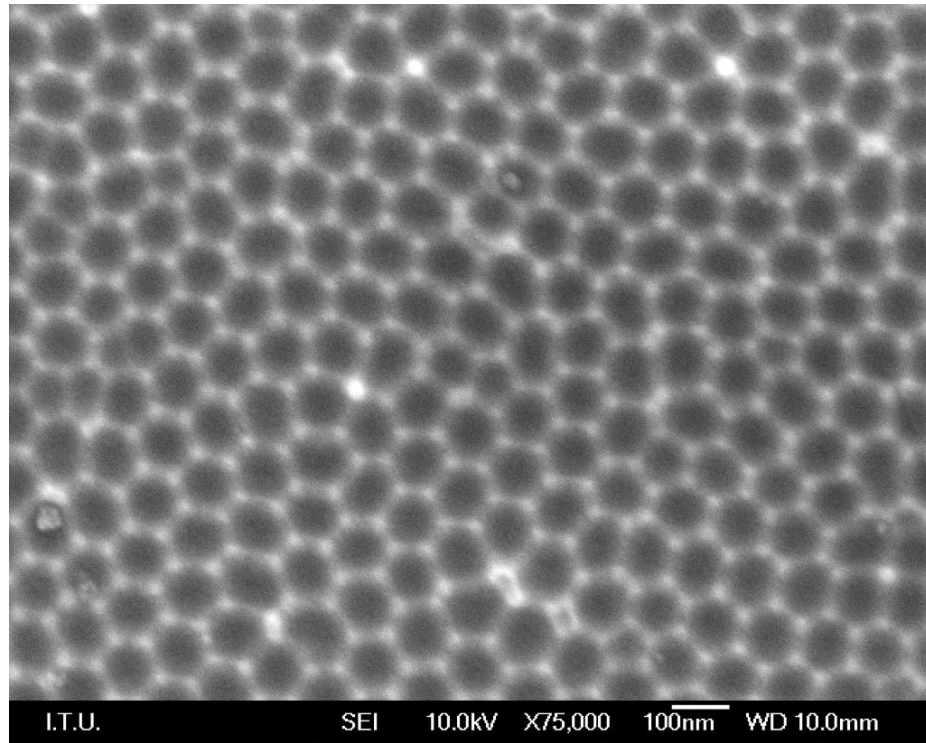


**Figure 5.3:** FEG-SEM image of the surface after the etching process at the end of the first step of anodization

Anodizing at 30V and 50V did not show a appreciable difference in the pore size, which was 24.5 nm (Figure 5.4.a) and 28 nm (Figure 5.4.b) respectively. However, anodizing in 70V showed a significant difference giving an average pore diameter of 51.6 nm (Figure 5.4.c). The AAO layer thickness also increased by increasing the applied potential. Anodizing at 30V for one hour produced AAO substrates with an average thickness of 1375 nm (Figure 5.5.a), whereas this value increased to 1615 nm by anodizing at 50V for 20 minutes (Figure 5.5.b) and to 2900 nm at 70V for 5 minutes (Figure 5.5.c).

The experiments performed at 5°C showed that increasing the applied voltage during anodizing also increased the pore diameter as well as the thickness. These results are in accordance with the previous studies present in the literature (Sulka, 2009).

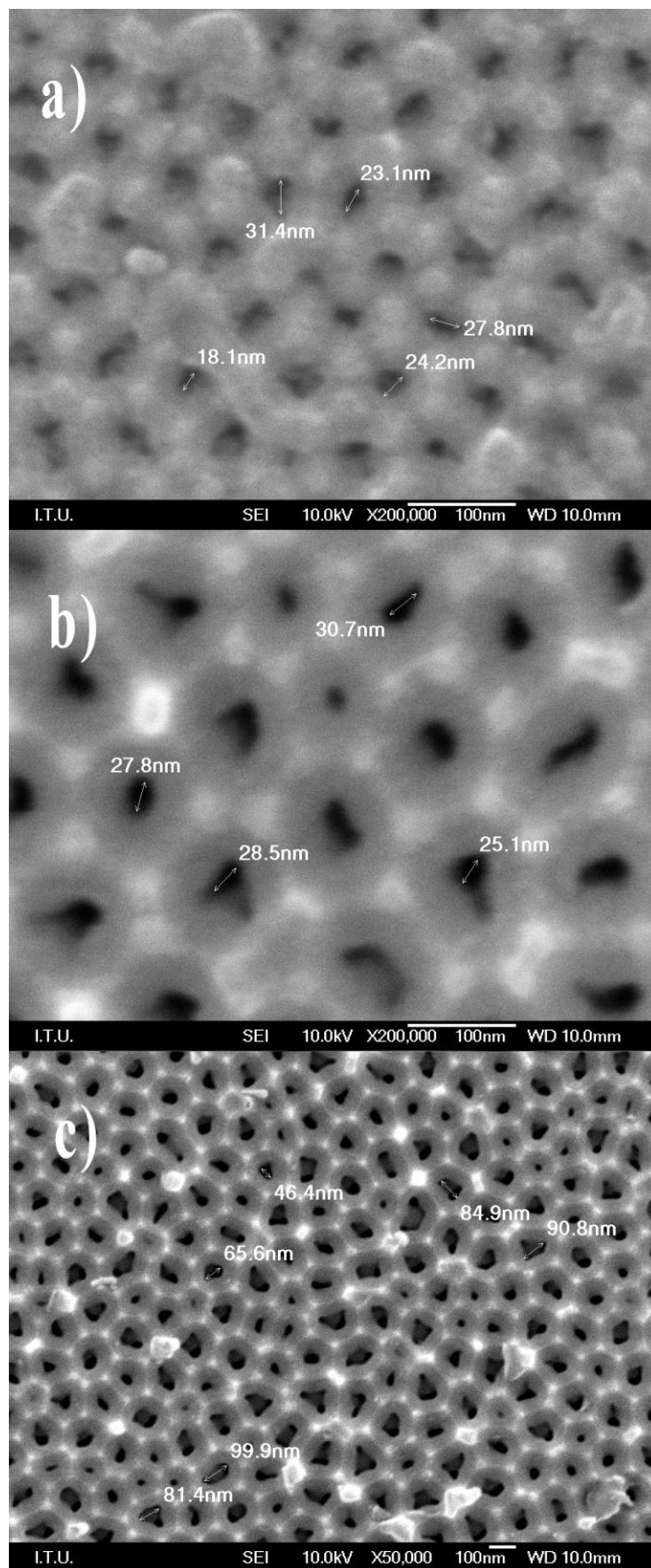


**Figure 5.4:** Pore diameters obtained by anodizing at 5°C at a) 30V, b) 50V, c) 70V

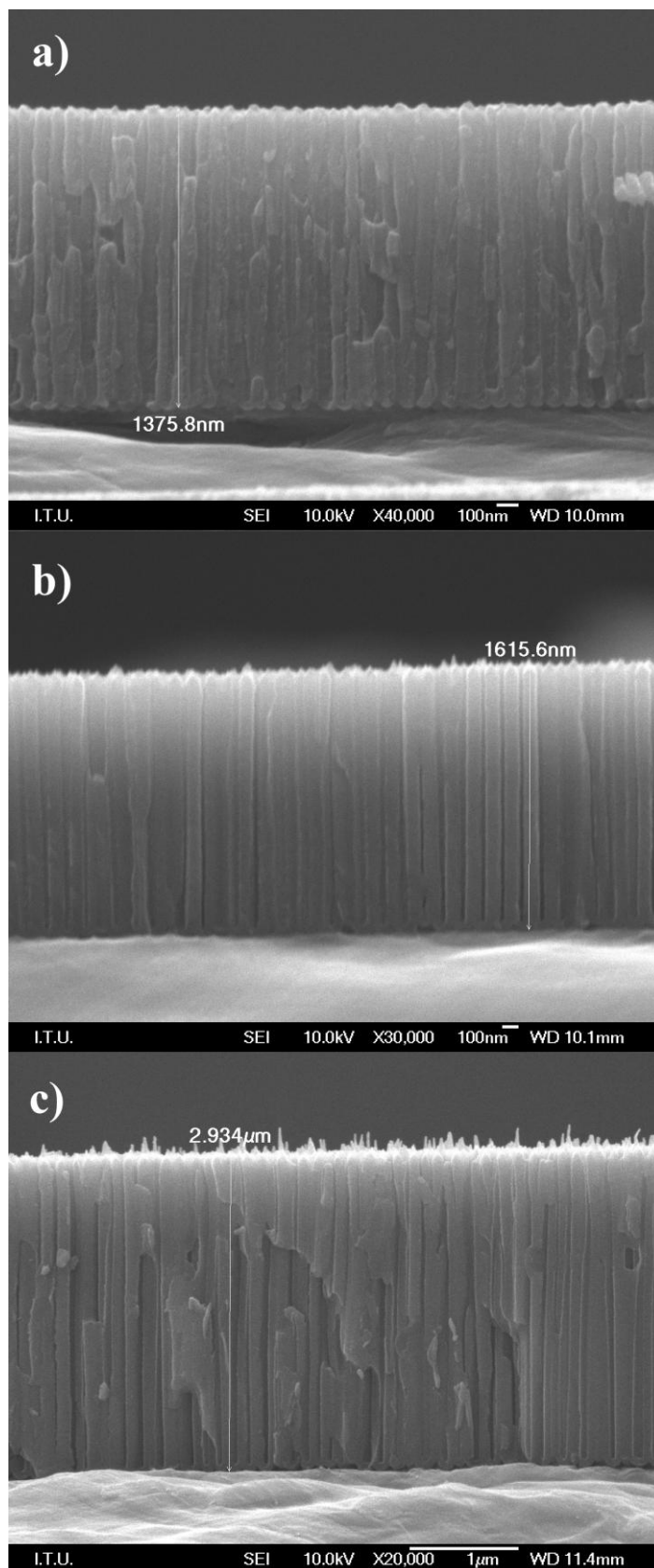


**Figure 5.5:** AAO thickness obtained by anodizing at 5°C at a) 30V, b) 50V, c) 70V

Same voltage levels (30V, 50V and 70V) were applied also at 25°C with the same etching procedure between the steps and the same agitation speed of 800 rpm.

The average pore diameters value of anodized aluminum in 30V at 25°C was around 24.8 nm (Figure 5.6.a); which was almost the same anodizing data obtained from 30V at 5°C. However, anodizing at 50V produced an average pore diameter of 59.4 nm (Figure 5.6.b), which is greater than 28 nm (50V at 5°C). The structure of the pores produced from 70V was different from the others, the porous structure is deteriorated due to the higher etching action of the electrolyte on the anodic oxide at higher temperatures and voltages. Therefore it was not possible to calculate an average pore diameter (Figure 5.6.c).

The AAO thickness values obtained from anodizing at 30V (Figure 5.7.a), 50V (Figure 5.7.b) and 70V (Figure 5.7.c) at 25°C, gave similar results in the sense of the effect of voltage increment on AAO thickness. Increasing voltage increased the anodizing rate.

The effect of temperature had great effect on the AAO growth rate. It was observed from the FEG-SEM pictures that increasing temperature for the same voltage values also increase the anodizing rate. The growth rates were calculated from the thickness values obtained from the FEG-SEM images. Table 5.1 shows the growth rates depending on the voltage and temperature values.

**Table 5.1:** Linear growth assumption of AAO layer in different parameters

	30V	50V	70V
5°C	1.37 µm/h	4.84 µm/h	35.20 µm/h
25°C	5.19 µm/h	11.46 µm/h	147.96 µm/h

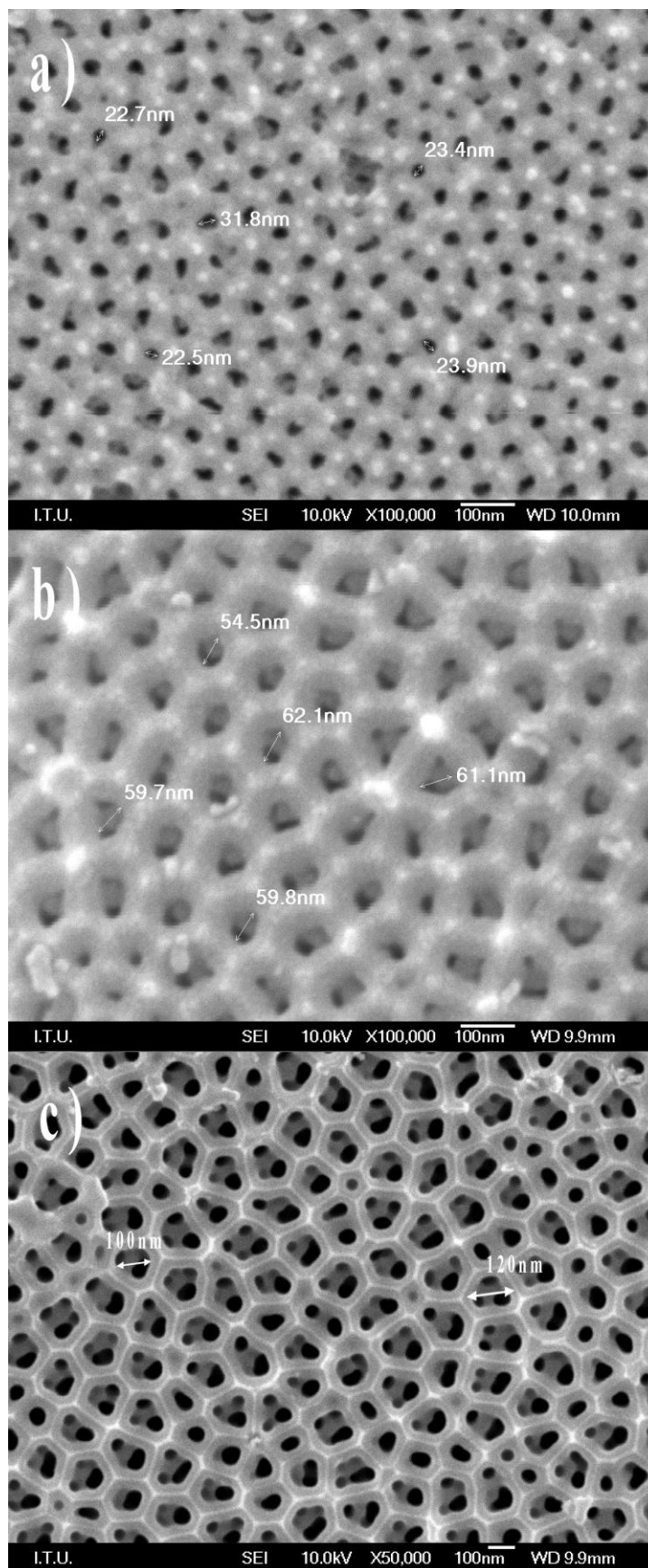


**Figure 5.6:** Pore diameters obtained by anodizing at 25°C at a) 30V, b) 50V, c) 70V

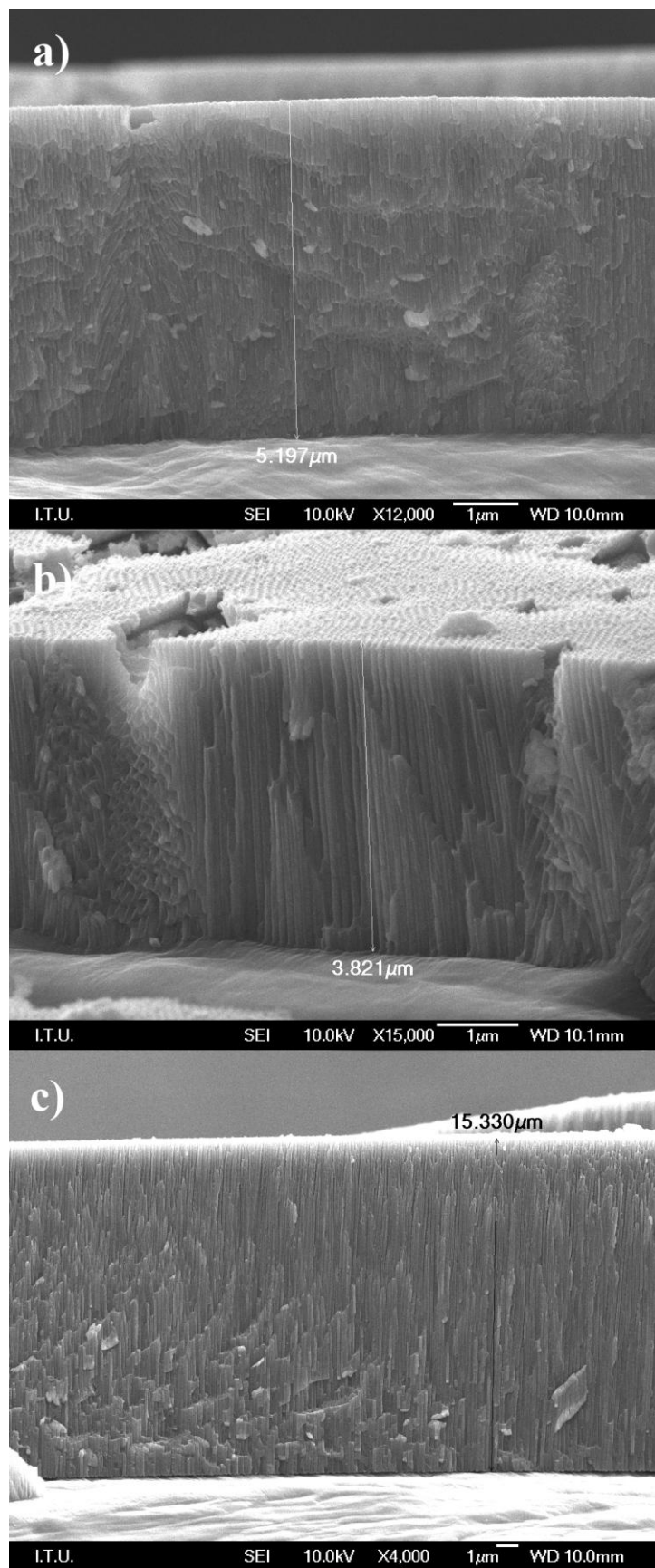


**Figure 5.7:** AAO thickness obtained by anodizing at  $25^{\circ}\text{C}$  at a) 30V, b) 50V, c) 70V

### 5.1.3 Optimization of AAO Substrates for the Production of Ni-W nanowires

After investigating the effects of applied voltage and anodizing temperature on AAO optimization studies were conducted for producing Ni-W nanowires having diameter around 100 nm and 2  $\mu\text{m}$ .

For the production of nanowires having diameter around 100 nm and 2  $\mu\text{m}$ , the first step of anodizing was needed to be chosen with parameters that could be easily controlled. Assuming that the further processes such as zincating as well as the acidic environment of electrolyte used in electrodeposition would increase the pore sizes, a pore diameter value that would be produced between 30V and 50V at 25°C could be satisfactory. Therefore, 40V was chosen as the first step of anodizing at 25°C. Anodizing was conducted in 800 rpm and then etched. Figure 5.8 shows the FEG-SEM image after the etching step.

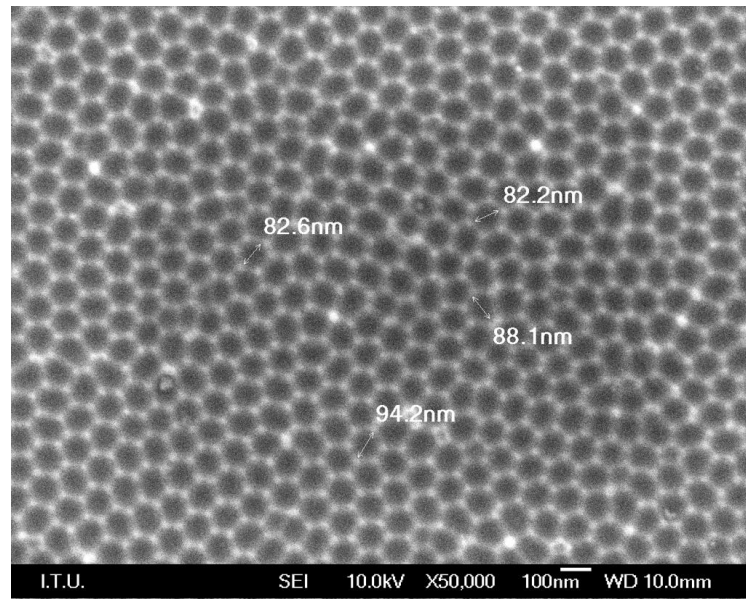


**Figure 5.8:** FEG-SEM image of the first step of anodizing at 40V at 25°C after etching

The second step needed to be a pore size controlled in order to grow columnar AAO layer enabling electrodeposition. It was observed in the previous experiments that 5°C provides a better pore size distribution than 25°C. Due to the fact that anodizing at 70V produces dimensions similar to the etched base, the second step was conducted under the conditions of 70V at 5°C (Figure 5.9). The inner diameters of the pores were around 20 nm which were enlarged afterwards.



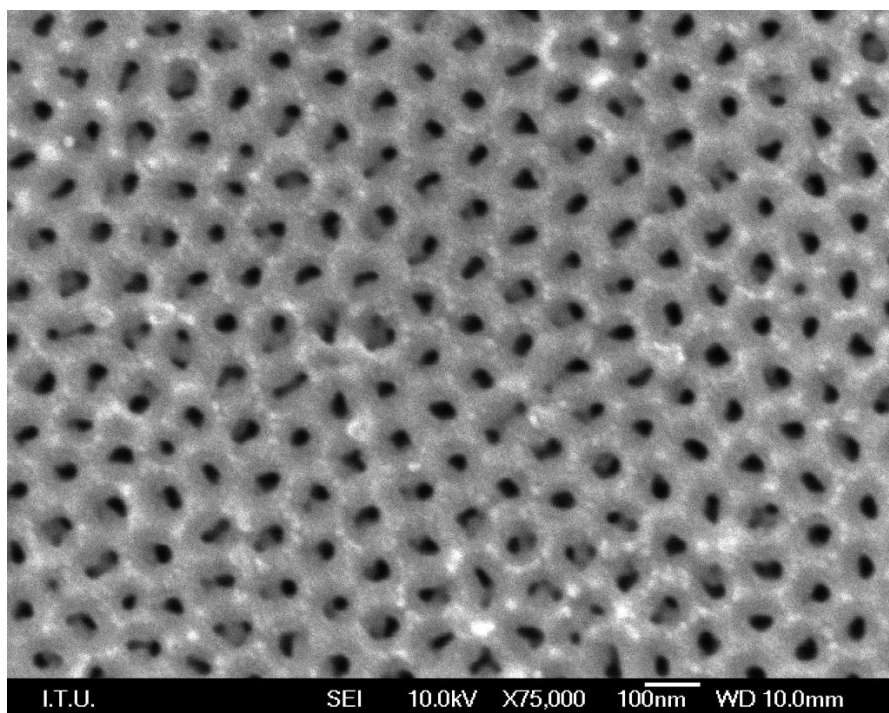


**Figure 5.9:** FEG-SEM image after the second step of anodizing

#### **5.1.4 Electrochemical Dissociation and Zincating**

After the second step of the anodization, electrochemical dissolution step was performed by reducing the voltage from 70 V to 15 V with the rate of 0.1 V/s by discussing the literature obtained (Saedi, 2005). After reaching 15 V, anodizing maintained for 30 minutes with the same temperature and agitation conditions. Figure 5.10.a shows the barrier layer which was produced by anodizing without electrochemical dissolution. It can clearly be seen in figure 5.8.b. that there are primary barrier layers deviating as branches through the Al base after electrochemical dissociation process. However it was not possible to eliminate the entire barrier layer.



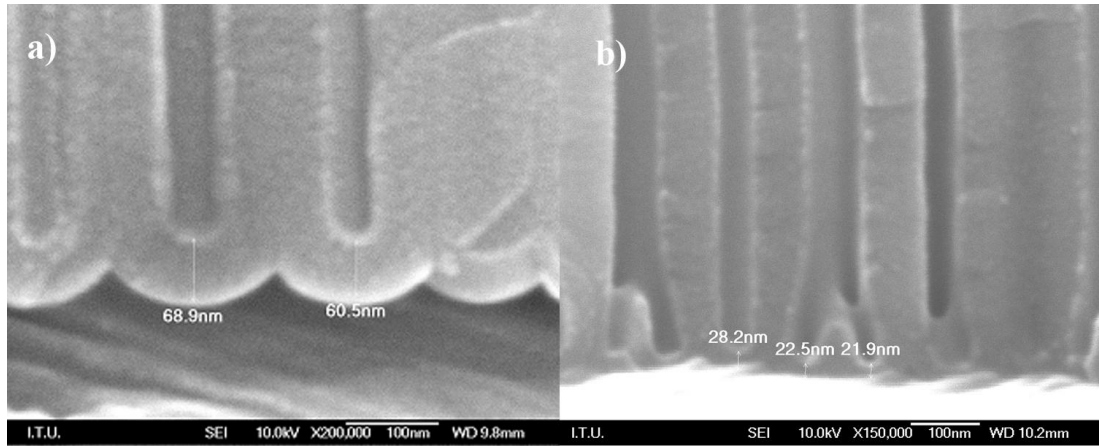


**Figure 5.10:** a) Barrier layer before electrochemical dissolution, b) after electrochemical dissolution

After the anodizing was finalized, the specimen was subjected to the zincate solution which was previously heated to 30-35 °C. Zincating duration was 25 seconds in ultrasonic cleaner. Figure 5.11.a shows the barrier layer after zincating process. It can be observed the the barrier layer was successfully eliminated and the bottom of the AAO pores and the substrates became ready for electrodeposition of Ni-W nanowires with the average diameter of 80 nm after being enlarged by the zincate solution due to the NaOH content. It is important to note that this value is very near the dimensions of the etched base previously shown in figure 5.8. Therefore it can be asserted that the pores were columnar and ideal for electrodeposition of Ni-W nanowires.

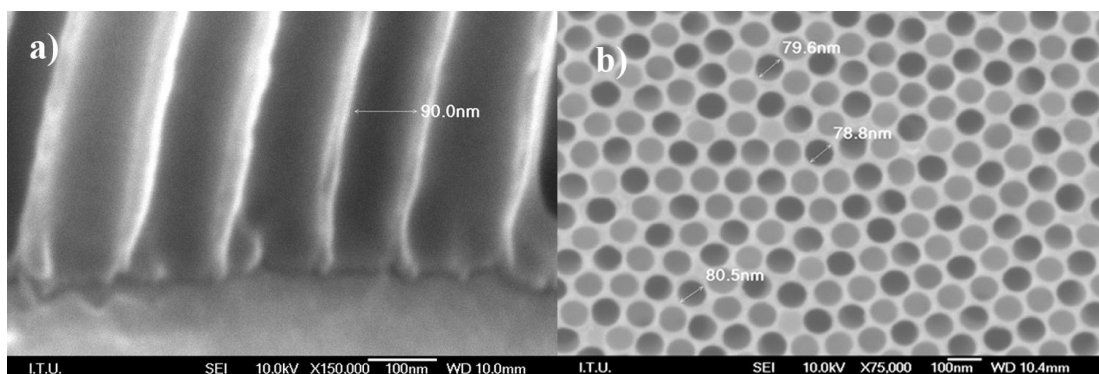


**Figure 5.11:** a) Cross section view, b) Top view of AAO after zincating

## 5.2 Electrodeposition of Ni-W Nanowires

In order to determine the ability of Ni-W deposition on zincated flat aluminum surfaces. Pure aluminum sheets were subjected to electrodeposition after zincating.

However, during electrodeposition of pore bottom activated AAO, it was observed that the optimum current density gap for Ni-W nanowire deposition was very narrow unlike the for Ni-W coatings on flat surfaces (Juskenas, 2008). The solution used contained 0.28 M citric acid acted as a complexing agent and set the pH value to 3, which was ideal for deposition inside the pores. When the electrolytes pH was higher than 3, highly probably the local pH increase within the pores led to nickel hydroxide precipitation leading to bad deposit quality. Decreasing the pH below 3 led to the rapid dissolution of AAO layer on Al, which took place faster than the electrodeposition of nanowires.

Deposition temperature is also another important criteria for electrodeposition on AAO because increased temperatures may lead to closure of pore by a mechanism similar to sealing. In contrary, low temperature leads to low faradaic efficiency that affects the charge transport in a negative way. Therefore, 60°C was selected as the deposition temperature.

Choosing the current density value lower than 1.25 A/dm<sup>2</sup> was not found to be adequate for uniform nanowire deposition. On the other hand, choosing 2.5 A/dm<sup>2</sup> (applied potential difference above 3.3 V) caused possible different hydroxide compounds of Ni to precipitate over the pores of AAO and to block further deposition related to local alkalization inside the pores similar to deposition experiments in higher pH levels than 3. It is important to note that the main reason for the limiting range of both pH and current density in homogeneous electrodeposition was the limited area on the bottom of the pores when compared to flat surfaces. This discussion agrees with the literature obtained on electrodeposition of Ni-W on flat surfaces (Juskenas, 2006).

Figure 5.12 demonstrates the voltage drop versus time, which is related to the deposition inside the pores of AAO. It can be realized from the figure that, increasing the current density also increases the deposition rate inside the pores since the voltage drop occurs faster in samples deposited with higher current densities. For

instance, selecting  $1.25 \text{ A/dm}^2$  filled the pores 20 minutes whereas by depositing in  $2.18 \text{ A/dm}^2$  this time period was reduced to 10 minutes.

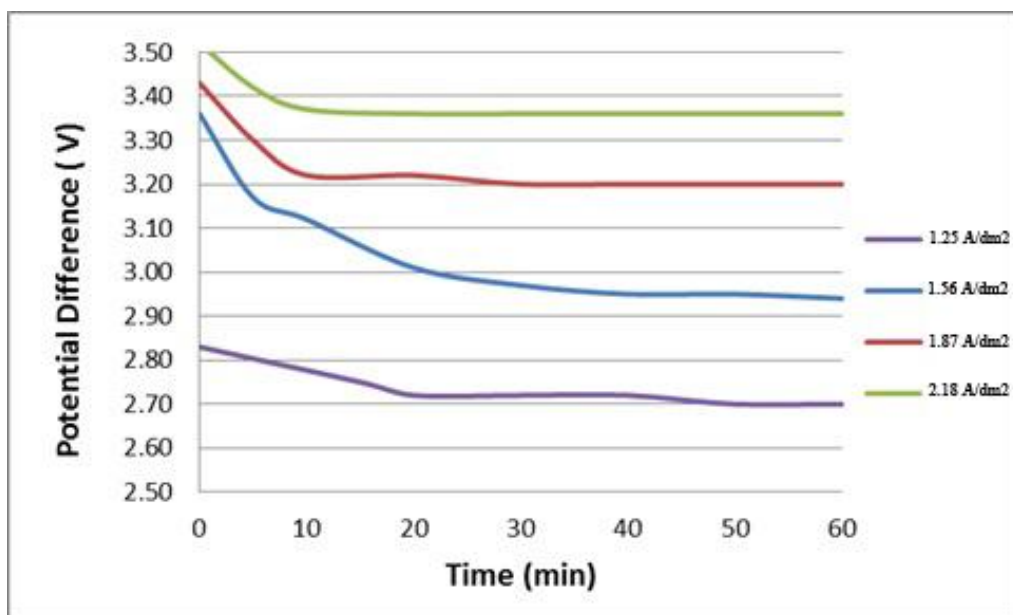


**Figure 5.12:** Cell Potential vs. time during electrodeposition of Ni-W nanowires

After the dissolution of samples in NaOH solution, some nanowires were separated from their base during fracturing for cross sectional investigations. In the samples produced by using  $1.25 \text{ A/dm}^2$ ,  $1.87 \text{ A/dm}^2$  and  $2.18 \text{ A/dm}^2$  (Figures 5.13.a and 5.13.b) this effect is very pronounced indicating the brittle structure of the wires produced under these conditions. The optimum properties with respect to durability during fracturing of free standing Ni-W structures was obtained when a current density of  $1.56 \text{ A/dm}^2$  was used during deposition (Figure 5.14).

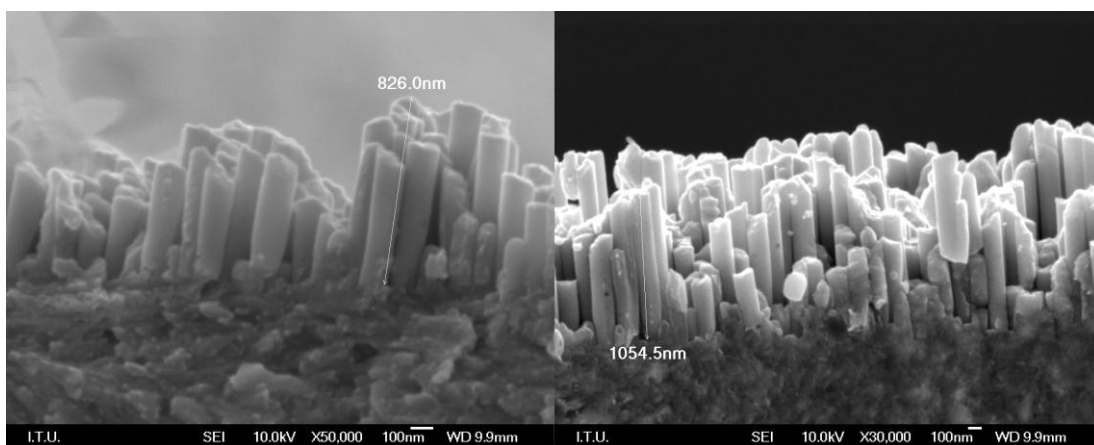


**Figure 5.13:** FEG-SEM images of Ni-W nanowires obtained in a)  $1.87 \text{ A/dm}^2$  and b)  $2.18 \text{ A/dm}^2$

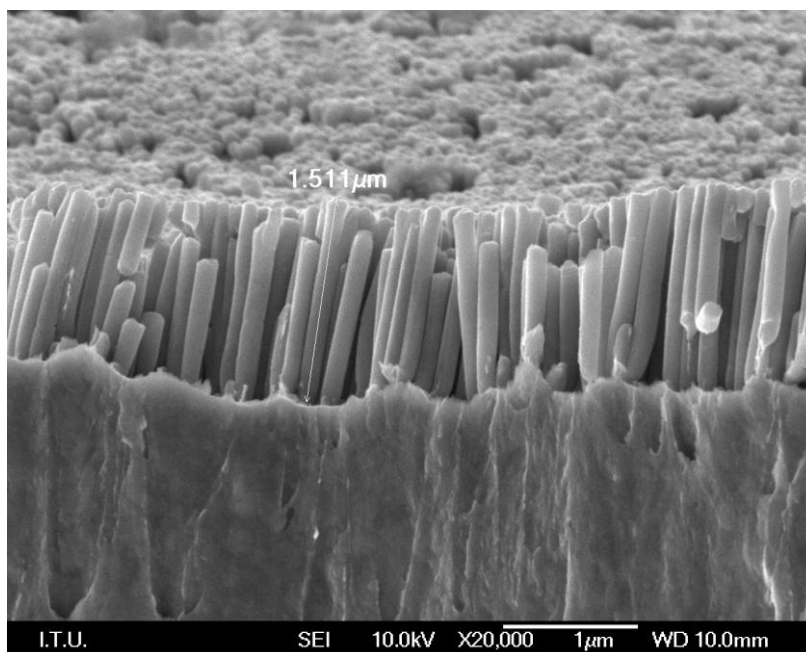


**Figure 5.14:** FEG-SEM image of electrodeposited Ni-W nanowires deposited in  $1.56 \text{ A/dm}^2$

The average length and diameters of Ni-W nanowires ranged in between 1.5 to 1.8  $\mu\text{m}$  and 120 to 140 nm respectively. From the figure 5.14 it can be asserted that the pores were entirely filled during electrodeposition.

The diameters of nanowires produced under different current densities did not show any appreciable dependence to current density (Figures 5.15 and 5.16). The diameters of the nanowires were around 130 nm for all the specimens. Only the nanowires produced under  $1.25 \text{ A/dm}^2$  gave a powdery nodular structure (Figure 5.15 a)

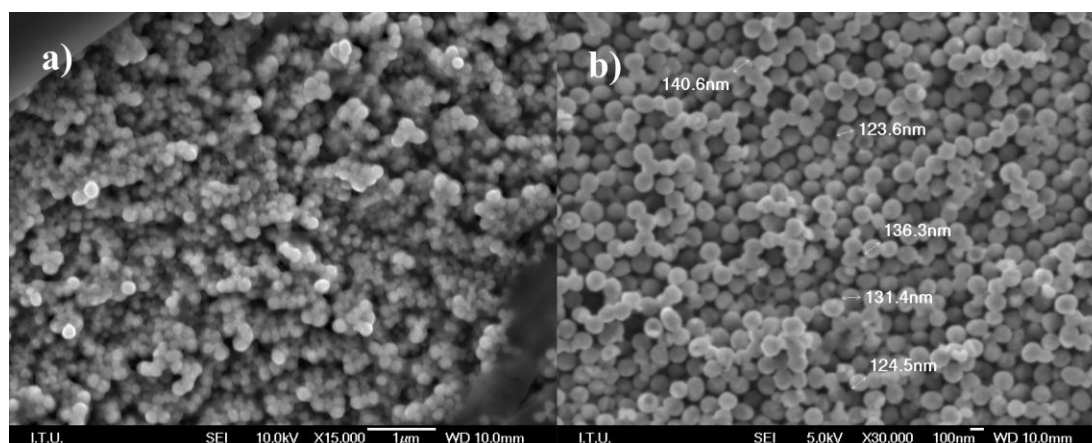


**Figure 5.15:** FEG-SEM images taken from the top view of deposits a)  $1.25 \text{ A/dm}^2$  and b)  $1.56 \text{ A/dm}^2$

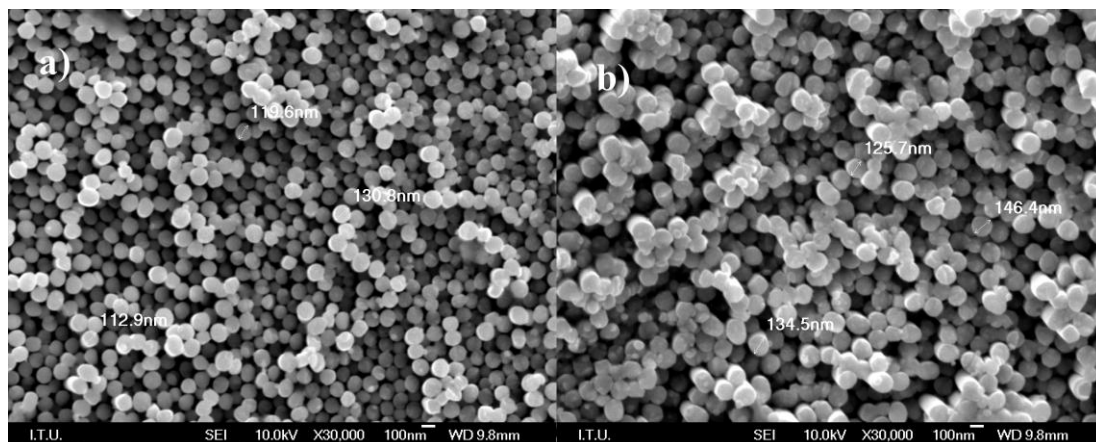


**Figure 5.16:** FEG-SEM Images taken from the top view of deposits a)  $1.87 \text{ A/dm}^2$  and b)  $2.18 \text{ A/dm}^2$

The EDS analyses (Figure 5.17) showed that the W content of all nanowires was around 9 %at which is in the solid solution region in the phase diagram of Ni-W (Figure 5.19). Some remnant Na was observed in the EDS spectrum of sample obtained by using  $1.25 \text{ A/dm}^2$  arising from insufficient rinsing.

After the EDS analyses, XRD patterns were obtained from the samples deposited in  $1.25 \text{ A/dm}^2$  (0.2A),  $1.56 \text{ A/dm}^2$  (0.25A),  $1.87 \text{ A/dm}^2$  (0.3A) and  $2.18 \text{ A/dm}^2$  (0.35 A).

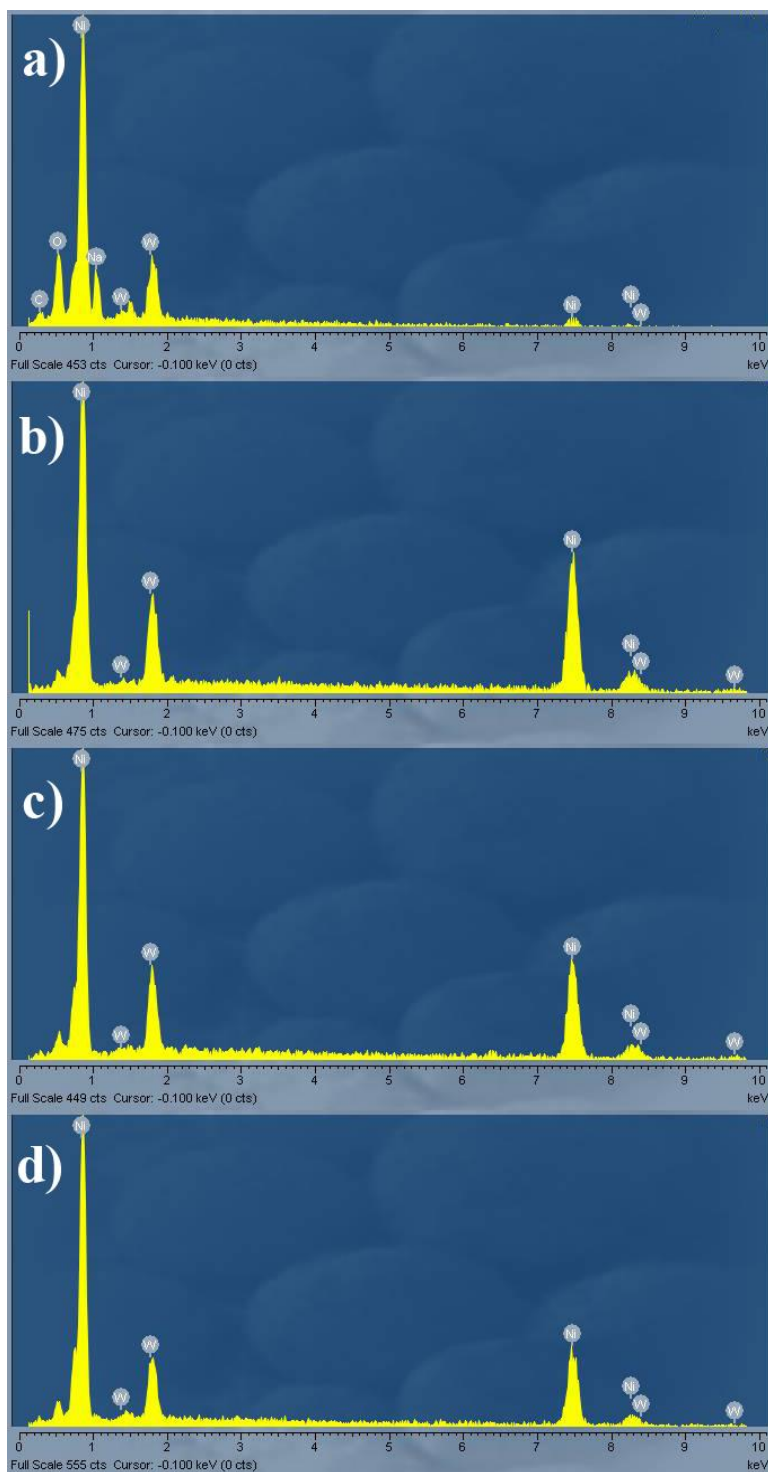


**Figure 5.17:** EDS patterns of samples deposited in 1.25 A/dm<sup>2</sup>, 1.56 A/dm<sup>2</sup>, 1.87 A/dm<sup>2</sup> and 2.18 A/dm<sup>2</sup>

For comparison, electrodeposited Ni and Ni-W coatings obtained on zincated Al were also subjected to XRD measurements (Figure 5.18).

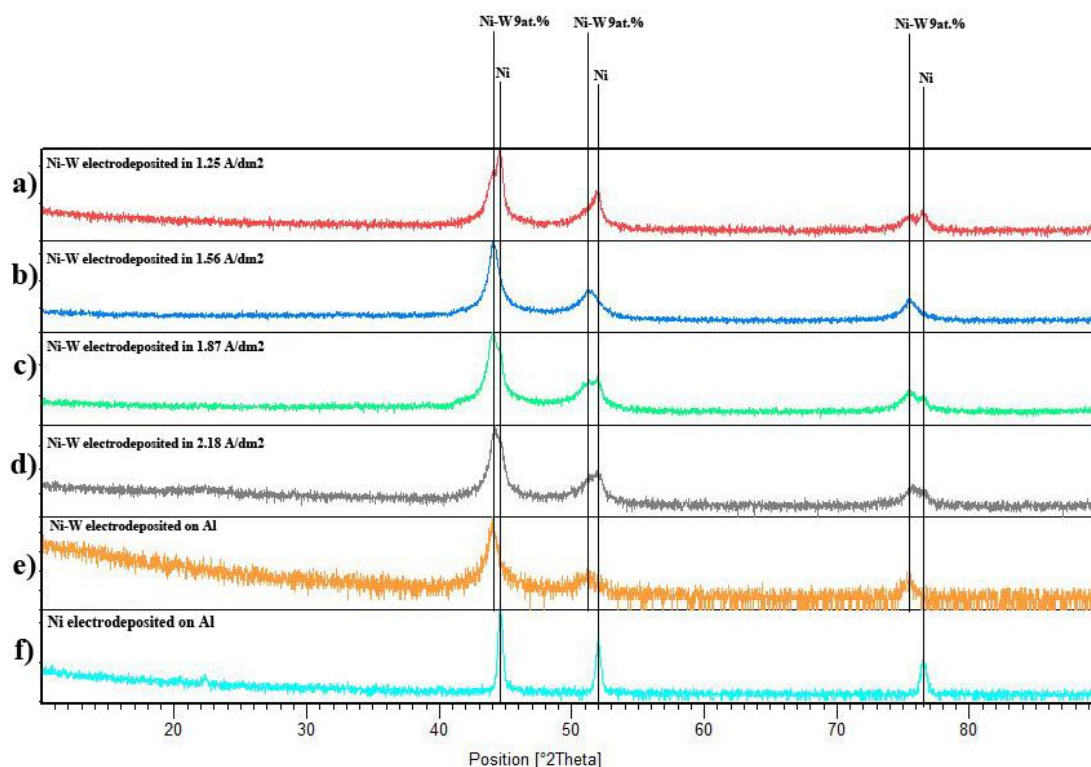


**Figure 5.18:** XRD patterns of Ni-W nanowires a) 1.25 A/dm<sup>2</sup>, b) 1.56 A/dm<sup>2</sup>, c) 1.87 A/dm<sup>2</sup>, d) 2.18 A/dm<sup>2</sup>, e) Ni-W on Al and f) Ni on Al

In patterns of electrodeposited Ni (Fig 5.18.f) specific peaks of Ni arising from (111), (200) and (220) characteristic planes can be seen at 45°, 52° and 77° respectively, as expected.

The XRD pattern of Ni-W on flat Al showed that the characteristic peaks of Ni is shifted to the left and broadened. The shift with respect to the positions of metallic nickel are due to the lattice expansion that occurred through the presence of W in solid solution with nickel. The broadening of the peaks took place as a result of nanocrystallization resulting from the presence of W in the structure (Watanabe, 2004).

In the XRD spectra of Ni-W nanowires peaks of Ni-W solid solution are clearly observable. The positions of the NiW solid solution did not show a difference with respect to their position when compared to the coating produced on flat aluminum. there are two peaks near the characteristic peaks of nickel.

However, in the XRD spectra of the nanowire samples obtained by using 1.25, 1.87 and 2.18 A/dm<sup>2</sup> additional metallic nickel peaks were also present. In the experimental part, it was previously mentioned that after filling the pores of AAO



with Ni-W the deposition is continued for obtaining a continuous layer of NiW alloys on their top. This process helped us to achieve a free standing structure that can easily be handled after removal of remnant aluminum and AAO. The layer covering NiW nanowires were further thickened in Watts solution by the electrodeposition of Ni. The reason for using Watts solution for further thickening was the high rate of deposition of metallic nickel from this solution. The metal nickel peaks observed in some of the XRD spectra of Ni-W nanowires are due to the diffractions arising from metallic nickel electrodeposited. However, in the sample electrodeposited in  $1.56 \text{ A/dm}^2$  these peaks cannot be seen, highly probably due to the high durability of these samples since detachment of Ni-W nanowires were not encountered during handling as observed in the FEG-SEM investigations (Figure 5.14).

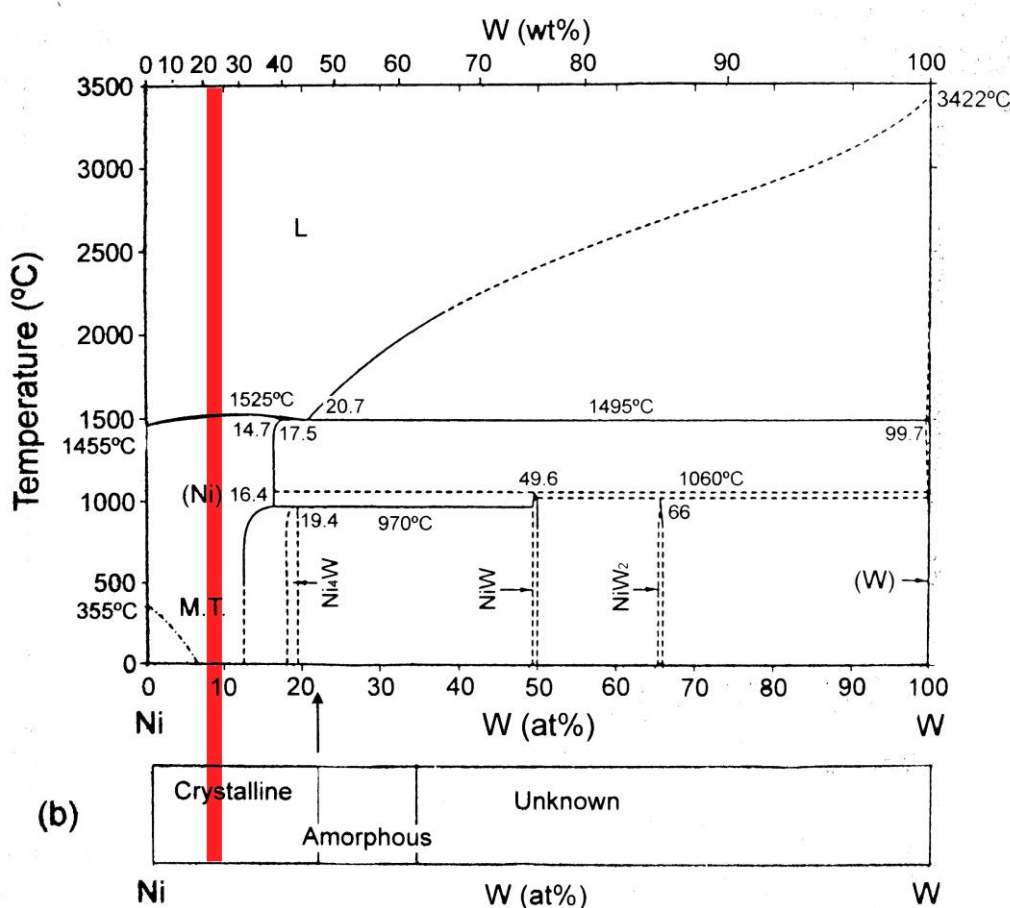


**Figure 5.19:** Ni-W phase diagram (Watanabe, 2004)



### 5.3 Electrocatalytic Properties of Ni-W and Ni-W Nanowires

In the literature there are studies (Krolikovski, 2009; Mitov, 2008) mentioning about the ability of increasing the electrocatalytic activity of nickel through alloying with W. In these studies the most pronounced catalytic activity increase was observed when Ni-W is in the solid solution state (up to 10 at%) (Hukovic, 2010). In this part of the study the possibility of further increasing the electrocatalytic activity of Ni-W alloys towards hydrogen evolution in alkaline environments by using them in nanowire form (benefiting from increase in surface area) is investigated. For this evaluation, flat nickel and Ni-W deposited samples and free standing Ni-W nanowire samples were used. The free standing Ni-W nanowires were produced under optimum conditions defined in section 5.2; namely by using a current density of 1.56 A/dm<sup>2</sup>.

The results of experiments conducted on flat nickel and nickel –tungsten alloy electrodeposits clearly indicated the promoting effect of W alloying on hydrogen evolution reaction (fig 5.20). The Tafel slopes and  $i_0$  values obtained from the cathodic polarization curves of these samples were 123 mV/dec and  $8 \cdot 10^{-5}$  A/cm<sup>2</sup> and 88 mV/dec and  $4 \cdot 10^{-4}$  A/cm<sup>2</sup> respectively. These values prove that Ni-W coatings have a better catalytic activity for H<sub>2</sub> evolution in alkaline solutions

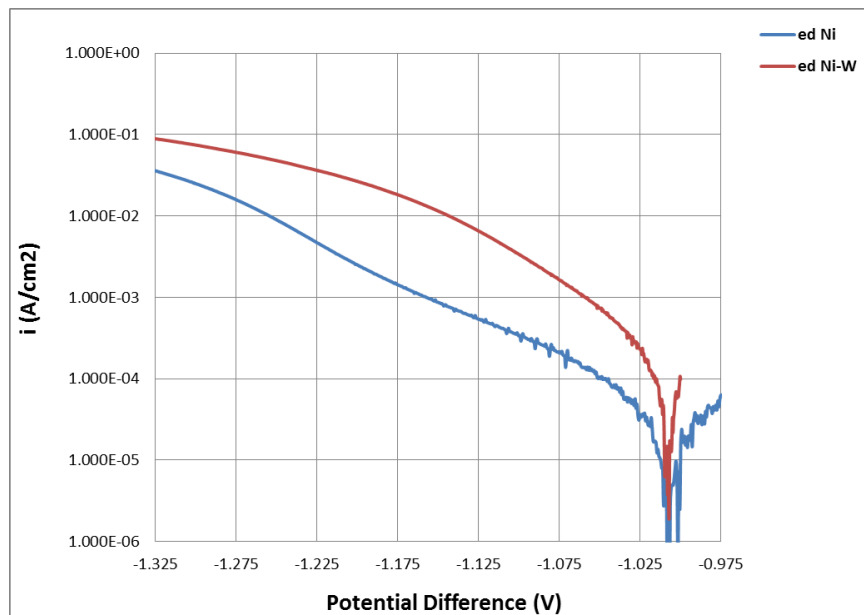


**Figure 5.20:** Polarization curves of electrodeposited Ni and Ni-W on Al

After comparing electrodeposited Ni-W to electrodeposited Ni, Ni-W nanowires were also tested for their catalytic activity. Figure 5.21 shows the polarization curve obtained from Ni-W nanowires. It is important to note that open circuit potential of the sample was -0.6V, which is below the reversible  $H^+/H_2$  potential is ( $E_{rev}(H^+/H_2) = -1.01 \text{ V vs Ag/AgCl}$ ). The Tafel slope of the sample obtained from the 50 mV more negative region of -1.01 V (beginning potential of hydrogen evolution reaction) gave a Tafel slope of 156 mV/dec. A lower open circuit potential than reversible potential for hydrogen evolution and high Tafel slope highly probaly indicates that the sample is covered with an oxide layer which is commonly observed in valve metals such as Ta, Nb, Ti, W, Zr and Ni based catalysts (Hukovic, 2006). The presence of a thin oxide or hydroxide layer on the surface of Ni-W may result from the deposition conditions with in the AAO pores or the alkaline dissolution process applied for the removal of aluminum and AAO from the structure. Further experiment and characterizaiton is required for the clarification the formation of these oxide structures on nanowires.

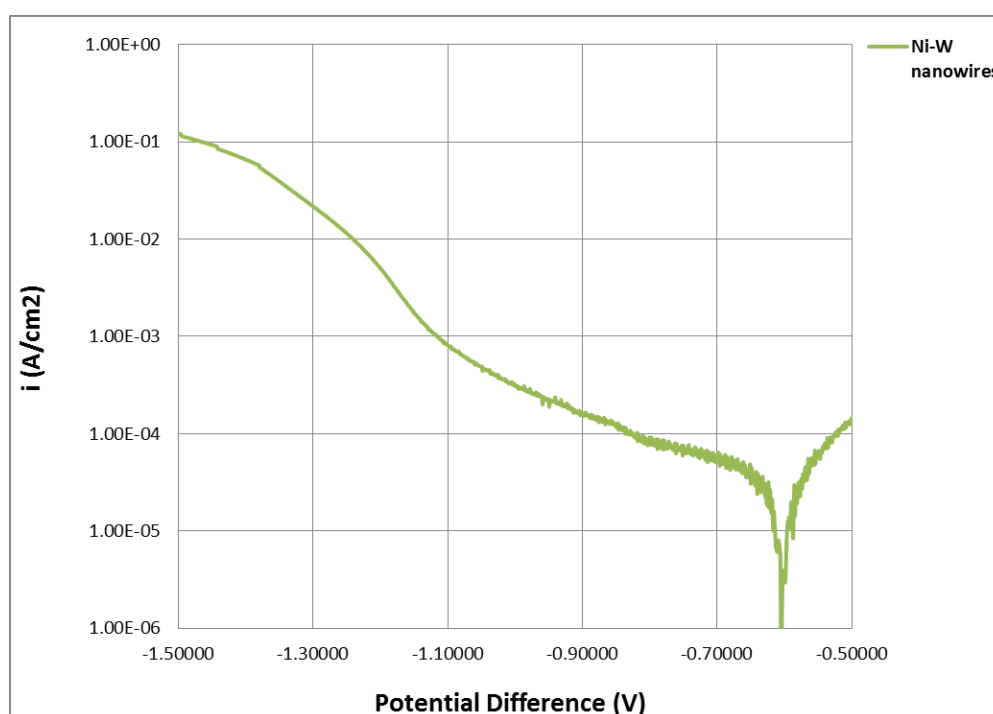


**Figure 5.21:** Polarization curve of Ni-W nanowires electrodeposited in  $1.56 \text{ A/dm}^2$

In conclusion, it was demonstrated that Ni-W surfaces can be utilized as electrocatalysts due to their low tafel slope and  $H_2$  evolution rate compared to pure Ni. It is predicted that if the formation of the oxide layer is avoided, the Ni-W

nanowires may lead to even higher H<sub>2</sub> evolution rate due to their increased contact surface which was not obtained in the present work.



## 6. CONCLUSIONS

In this study free standing Ni-W nanowires were produced for the first time by the electrodeposition of Ni-W alloys into the pores of AAO templates after a special pore bottom activation process.

- It was observed from the FEG-SEM images that electropolishing has an important effect on smoothening the surface of AAO templates for better Ni-W nanowire deposition.
- Two step anodization has a great effect on hexagonal arrangement of the pores in AAO membranes compared to one step anodization. According to the experiments performed at 30V, 50V and 70V, increasing the anodization voltage is directly proportional to the pore size and final thickness of AAO templates obtained. Moreover, increasing the temperature also has the similar effect as voltage increment, which is more significant in elevated values of applied voltage during anodizing.
- The experiments showed that the optimum pore ordering was obtained by the hybrid method of anodizing, performed in 40V 25°C for one hour and then 70V 5°C for five minutes as the second step. The pore diameters obtained was 20nm and the thickness of the AAO layer was 2  $\mu\text{m}$ . It should be noted that the desired nanowire length can be adjusted by changing the duration of the second step. It can also be noted that cold anodizing has a significant advantage in the sense of thickness control.
- Electrochemical dissolution method was found to be a useful method for making the barrier layer thinner. However, zincating was necessary in order to achieve entire elimination which was successfully applied to the substrates prior to electrodeposition of Ni-W nanowires.
- Free-standing Ni-W nanowires were successfully produced by electrodeposition which had a specific deposition current density value around 1.56 A/dm<sup>2</sup>. It was not possible to obtain uniform deposition in 1 A/dm<sup>2</sup> and

current densities over  $2.5 \text{ A/dm}^2$  caused closure of pore tips with probable hydroxide precipitation.

- Changing current density for electrodeposition didn't cause a significant W content in the structure; since the optimum current range is not wide compared to electrodeposition process on flat surfaces.
- FEG-SEM images revealed that the pores of AAO were successfully filled with Ni-W nanowires according to the thickness of AAO membrane and the length of deposits. The average length of nanowires were around 1.5-1.8  $\mu\text{m}$  and the diameters ranged from 120 nm to 140 nm. The diameter of zincated AAO membranes and the nanowires are totally identical due to the effect of aggressive character of the deposition environment on AAO. If the conductivity of the electrolyte is increased, separately distributed of wires can be obtained with diameter values closer to the pore diameter of AAO. For further research, different complexing agents may be utilized with higher pH values in the electrolyte which would be less destructive for the AAO and might also supply sufficient charge transfer.
- According to the XRD patterns obtained from the analyses broadened and shifted characteristic peaks of Ni in (111), (200) and (220) were observed. Additionally, after investigating Ni-W coatings on Al, the characteristic peaks of Ni were shifted to the left side of the patterns with broader structure due to the decrease of crystallinity. As the W was dissolved in the solid solution, the crystallinity was decreased and the peaks were shifted due to the enlargement of the lattice structure. These findings fit well with the literature. On the other hand, all the nanowire samples (except the one electrodeposited in  $1.56 \text{ A/dm}^2$ ) showed two peaks around the characteristic peaks of Ni. They both belonged to Ni and Ni-W due to the detachment of wires and the elemental structure of the deposit from the Watts solution. In contrast, electrodepositing nanowires in  $1.56 \text{ A/dm}^2$  did not lead to structure deficiencies in Ni-W nanowires. Therefore we did not encounter pure Ni peaks in the XRD patterns.
- The polarization curves showed that Ni-W nanowires have a potential to be used as electrocatalysts as an alternative to pure Ni or Ni-W coatings. The

different open circuit potential of Ni-W nanowires electrodeposited in 1.56 A/dm<sup>2</sup> may be explained by residual oxide compound formation on the nanowire structures which affected the electrocatalytic activity in a negative way. In the next experiments it is reasonable to predict that longer nanowires may lead to even more rapid H<sub>2</sub> evolution with respect to the increment in contact area.

- In conclusion was demonstrated that Ni-W coatings can be utilized as electrocatalysts due to their low tafel slope and H<sub>2</sub> evolution rate compared to pure Ni. It is estimated that if the possible oxide layer is avoided, the Ni-W nanowires may lead to even higher H<sub>2</sub> evolution rate due to their increased contact surface area.





## REFERENCES

- Alkan, B.**, 2009, İndium Antimonid (InSb) Nano Tellerin Elektrolitik Alaşım Biriktirme Yöntemiyle Üretilmesi ve Karakterizasyonu, *MSc. Thesis*, Istanbul Technical Univesity, Istanbul, Turkey
- Alpay, N.**, 2009, Farklı Önişlem Yöntemlerinin Alüminyum Anodizasyonu Üzerindeki Etkisi, *MSc. Thesis*, Istanbul Technical Univesity, Istanbul, Turkey
- Bandyopadhyay, S. and Nalwa, H. S.**, 2003, Quantum Dots and Nanowires, American Scientific Publishers, USA
- Bhushan, B.**, 2004, Nanowires, *Springer Handbook of Nanotechnology*, pp. 99-138, Springer-Verlag Berlin Heidelberg, Germany
- Cadena, J. G., Comini, E., Ferroni, M., Vomiero, A. and Sberveglieri, G.**, 2010, Synthesis of different ZnO nanostructures by modified PVD process and potential use for 1dye-sensitized solar cells, *Materials Chemistry and Physics* **124**, pp. 694–698
- Cao, G. and Liu, D.**, 2008, Template-based synthesis of nanorod, nanowire, and nanotube arrays, *Advances in Colloid and Interface Science*, **136**, pp. 45–64
- Cheng S. L. and Huang C. N.**, 2008, Template Synthesis of Large-Scale Single-Co-Ni Alloy Nanowire Arrays by Electrochemical Deposition, Synthesis and Reactivity in Inorganic, *Metal-Organic, and Nano-Metal Chemistry*, **38**:6,475-480.
- Chianpariot, A., Lothongkum, G. and Schuh, C. A.**, 2011, Corrosion of nanocrystalline Ni-W alloys in alkaline and acidic 3.5 wt. % NaCl solutions
- Delgado, G.C.**, 2010, Economics and Governance of Nanomaterials: Potential and Risks, *Technology in Society*, **32**, pp.137-144
- Eliaz, N., Sridhar, T. M. and Gileadi, E.**, 2005, Synthesis and characterization of nickel tungsten alloys by electrodeposition, *Electrochimica Acta*, **50**, pp.2893- 2904
- Hamrakulov, B., Kim, I., Lee, M. G. and Park, B. H.**, 2009, Electrodeposited Ni, Fe, Co and Cu single and multilayer nanowire arrays on anodic aluminum oxide template, *Trans. Nonferrous Met. Soc. China*, **19**, pp. 83-87
- Haruyama, J., Davydov, D.N., Roukevich, D., Ellis, D., Statt, B.W., Moskovits, M. and Xu, J.M.**, 1998, *Solid State Electron*, **42**, p1257.
- Heremans, J. and Thrush, C. M.**, 2000, Bismuth nanowire arrays: synthesis and galvanomagnetic properties, *Phys. Rev., B* **61**, pp. 2921–2930
- Huber, C.A., Huber, T.E., Sadoqi, M., Lubin, J.A., Manalis, S. and Prater, C.B.**, 1994, *Science*, **263**, p800

- Hukovic, M. M., Grubac, Z., Radic, N. and Tonejc, A.,** 2006, Sputter deposited nanocrystalline Ni and Ni-W films as electrocatalysts for hydrogen evolution, *Journal of Molecular Catalysis A: Chemical*, **249**, pp.172- 180
- Islam N. and Miyazaki K.,** 2010, An empirical analysis of nanotechnology research domains, *Technovation*, **30**, pp. 231-235
- Jagminas, A., Kurtinaitiene, M., Angelucci, R. and Valincius, G.,** 2005, Modification of alumina barrier-layer through re-anodization in an oxalic acid solution with fluoride additives, *Applied Surface Sciences*, **252**, pp. 2360-2362
- Jin, J. G., Lee S.K. and Kim, Y. H.,** 2004, Adhesion improvements electroless Ni layer by ultrasonic agitation during zincating process, *Thin Solid Films*, **466**, pp. 272-278
- Juskenas, R., Valsunas, I., Pakstas, V. and Giraitis, R.,** 2009, On the state of W in electrodeposited Ni–W alloys, *Electrochimica Acta*, **54**, pp.2616-2620
- Karahasanoglu, C.,** 2009, Nikel Nanotellerin Üretimi ve Karakterizasyonu, *MSc. Thesis*, Istanbul Technical University, Istanbul, Turkey
- Krolikovski, A. and Plonska, E.,** 2009, Effects of compositional and structural features on corrosion behavior of nickel-tungsten alloys, *J Solid State Electrochem*, **13**, pp.263-275
- Lillo, M. and Losic, D.,** 2009, Pore opening detection for controlled dissolution of barrier oxide layer and fabrication of nanoporous alumina with through-hole morphology, *Journal of Membrane Science*, **327**, pp. 11-17
- Lin, Y., Sun, F.K., Yuan, X. Y., Geng, B.Y. and Zhang, L. D.,** 2003, Sol–gel electrophoretic deposition and optical properties of Fe<sub>2</sub>O<sub>3</sub> nanowire arrays, *Appl. Phys.*, **A 78**, pp. 1197-1199
- Masuda, H. and Fukuda, K.,** 1995, *Science*, **268**, p1466
- Mengke, L., Chengwei, W. and Hulin, L.,** 2001, Synthesis of ordered Si nanowire arrays in porous anodic aluminum oxide templates, *Chinese Science Bulletin*, **Vol. 46 No. 21**, pp. 1793-1796
- Metzler, O. Y., Zhu, L., and Gileadi, E.,** 2003, The anomalous codeposition of tungsten in the presence of nickel, *Electrochimica Acta*, **48**, pp. 2551-2562
- Meyyappan, M. and Sunkara, M. K.,** 2010, Inorganic Nanowires-Applications, Properties and Characterization, CRC Press, USA
- Mitov, M., Hristova, E., Hristov, G., Rashkov, R., Arnaudova, M. And Popov, A.,** 2008, Catalytic activity of Ni-W electrodeposits, *Environ Chem Lett*, **7**, pp. 249-253
- Paunovic, M. and Schlesinger, M.,** 2006, Fundamentals of electrochemical deposition, Wiley-Interscience, USA
- Roco, M. C.,** 2010, A Long-Term View of Nanotechnology Development: The National Nanotechnology Initiative at Ten Years, p. 3-5, World Technology Evaluation Center (WTEC)

- Saedi, A. and Ghorbani, M.,** 2005, Electrodeposition of Ni–Fe–Co alloy nanowire in modified AAO template, *Materials Chemistry and Physics*, **91**, pp. 417-423
- Salamon, A. W., Courtney, P. and Shuttler, I.,** 2010, Nanotechnology and Engineered Materials: A Primer, p. 7, Retrieved 17.11.2010 from [http://courses.engr.uky.edu/CME/cme470/nanotechnology/PE\\_nanotechnologyprimeren.pdf](http://courses.engr.uky.edu/CME/cme470/nanotechnology/PE_nanotechnologyprimeren.pdf)
- Santos, A., Vojkuvka, Pallares, J., Ferre-Borrull, J. and Marsal, L. F.,** 2009, In situ electrochemical dissolution of the oxide barrier layer of porous anodic alumina fabricated by hard anodization, *Journal of Electroanalytical Chemistry*, **632**, pp. 139-142
- Sarkar, J., Khan, G. G. and Basumallik, A.,** 2007, Nanowires: properties, applications and synthesis via porous anodic aluminium oxide template, *Bull. Mater. Sci.*, **Vol. 30, No. 3**, pp. 271-290
- Shankar, K. S. and Raychaudhuri, A. K.,** 2005, Fabrication of nanowires of multicomponent oxides: Review of recent advances, *Materials Science and Engineering*, **25**, pp. 738-751
- Sheng, J., Yi, X. and Fang, W.,** 2010, Effects of tungsten on the catalytic activity of Ni–W catalysts for the hydrogenation of aromatic hydrocarbons, *React Kinet Mech Cat*, **99**, pp. 371-379
- Sriraman, K. R., Raman, S. G. S. and Seshadri, S. K.,** 2006, Synthesis and evaluation of hardness and sliding wear resistance of electrodeposited nanocrystalline Ni–W alloys, *Materials Science and Engineering*, **A 418**, pp. 303-311
- Su, Y., Shen, C., Yang, H., Li, H. and Gao, H.,** 2007, Controlled synthesis of highly ordered CuO nanowire arrays by template-based sol-gel route, *Trans. Nonferrous Met. SOC. China*, **17**, pp. 783-786
- Sulka, G. D., Stepniowski, W. J.,** 2009, Structural features of self-organized nanopore arrays formed by anodization of aluminum in oxalic acid at relatively high temperatures, *Electrochimica Acta*, **59**, pp. 3683-3691
- Urgen M., Yesil Y.,** 2009. Method for the Preparation of Nanostructures and Nanowires, PCT; PCT/US 2009/0229989.
- Url-1** <<http://en.wikipedia.org>>, accessed at 10.10.2010.
- Url-2** <<http://www.foresight.org/nano/history.html>>, accessed at 10.10.2010
- Url-3** <<http://whatis.techtarget.com>>, accessed at 07.11.2010
- Url-4** <<http://electrochem.cwru.edu>>, accessed at 08.12.2010
- Url-5** <<http://lh3.ggpht.com>>, accessed at 08.12.2010
- Url-6** <<http://www.rustyiron.com>>, accessed at 17.12.2010
- Volk, P.,** 2004, Zincate Treatment of Aluminium, *SurTech Technical Letter*, Chapter 15, pp. 1-10, retrieved from <[www.surtec.com/TB/TB15E.pdf](http://www.surtec.com/TB/TB15E.pdf)> on 17.11.2010
- Vradman, L. and Landau, L. D.,** 2001, Structure–function relations in supported Ni–W sulfide hydrogenation catalysts, *Catalysis Letters*, **77**, pp. 47-54

- Watanabe, T.**, 2004, Nanoplatting- Microstructure control theory of plated film and database of plated film structure, Elsevier
- Wagner, R. S. and Ellis, W. C.**, 1964, Vapor-liquid-solid mechanism of single crystal growth , *Appl. Phys. Lett.*, **4**, pp. 89-90
- Wang, N., Cai, Y. and Zhang, R. Q.**, 2008, Growth of nanowires, *Materials Science and Engineering*, **60**, pp. 1-5
- Wu, X. C. and Tao, Y. R.**, 2002, Growth of CdS nanowires by physical vapor deposition, *Journal of Crystal Growth*, **242**, pp. 309–312
- Xu, D., Xu, Y., Chen, D., Guo, G., Gui, L. and Tang, Y.**, 2000, *Chem. Phys. Lett.*, **325**, p340
- Xu, H., Qin, D. H., Yang, Z. and Li, H.L.**, 2003, Fabrication and characterization of highly ordered zirconia nanowire arrays by sol–gel template method, *Materials Chemistry and Physics*, **80**, pp. 524-528
- Yamasaki, T.**, 2001, high-strength nanocrystalline ni-w alloys produced by electrodeposition and their embrittlement behaviors during grain growth, *Scripta Mater.*, **44**, pp. 1402-1502

## **CURRICULUM VITAE**

Doğın Işıhan Paşaoğlu was born in Ankara, 1986. After graduating from Çankaya Milli Piyango Anatolian High School, he was accepted to Istanbul Technical University, for Metallurgical and Materials Engineering. He successfully got his bachelor's degree in 2008 and enrolled in double degree masters programme of Politecnico Di Milano and Istanbul Technical University on Materials Engineering.

### **Publications:**

- **Paşaoğlu, D. I.**, Eraslan, S., Sezgin, A., Aypar A., Kılıç, Y., 2008. Can Plants Synthesize Precursors for Nanoparticle Production?, *IV. Nanobilim ve Nanoteknoloji Konferansı*, Istanbul, Turkey, June 9-13.